iScience

CellPress
OPEN ACCESS

Article

Robust anti-SARS-CoV2 single domain antibodies cross neutralize multiple viruses

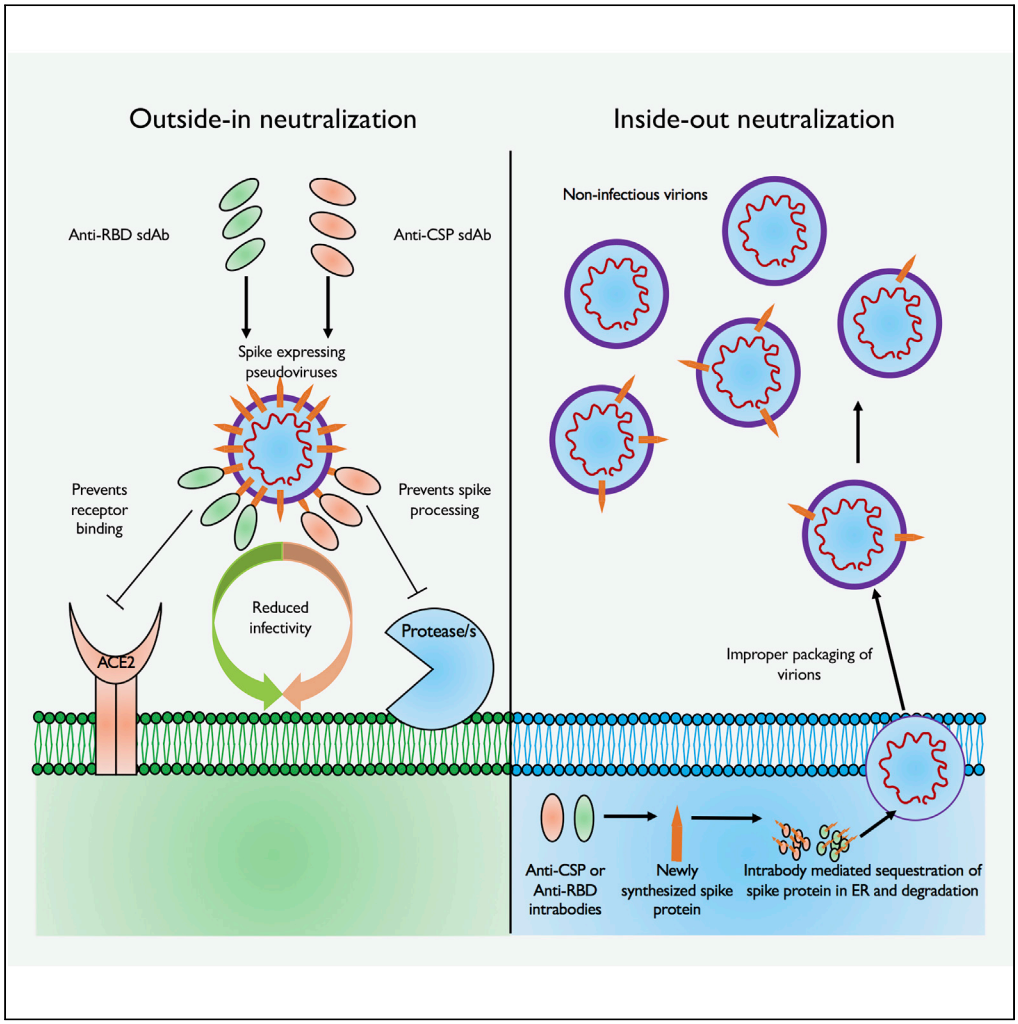

Sudhakar Singh, Surbhi Dahiya, Yuviana J. Singh, ..., Abhishek Dubey, Azeez Tehseen, Sharvan Sehrawat

sharvan@iisermohali.ac.in

Highlights

Anti-CSP and anti-RBD sdAb efficiently neutralized LV (SARS-CoV2 S) pseudoviruses

Both intrabodies prevented the biogenesis of SARS-CoV2-S pseudovirions

Anti-CSP sdAb neutralized viruses such as HSV1 and PPRV

Anti-HSV1 and anti-PPRV sera neutralized LV(CoV2 S) pseudoviruses

Singh et al., iScience 25, 104549
July 15, 2022
https://doi.org/10.1016/j.isci.2022.104549

iScience

CellPress
OPEN ACCESS

Article

Robust anti-SARS-CoV2 single domain antibodies cross neutralize multiple viruses

Sudhakar Singh,[1,2] Surbhi Dahiya,[1,2] Yuviana J. Singh,[1] Komal Beeton,[1] Ayush Jain,[1] Roman Sarkar,[1] Abhishek Dubey,[1] Azeez Tehseen,[1] and Sharvan Sehrawat[1,3,*]

SUMMARY

We report robust SARS-CoV2 neutralizing sdAbs targeting the viral peptides encompassing the polybasic cleavage site (CSP) and in the receptor binding domain (RBD) of the spike (S) protein. Both the sdAbs inhibited infectivity of the CoV2 S protein expressing pseudoviruses (LV-CoV2S). Both anti-CSP and RBD intrabodies (IB) inhibited the output of LV(CoV2 S). Anti-CSP IB altered the proteolytic processing and targeted the viral S protein for degradation. Because of cross-reactive CSPs in the entry mediators, the anti-CSP sdAb neutralized *in vitro* and *in vivo* the infectivity of SARS-CoV2 unrelated viruses such as herpes simplex virus 1 (HSV1) and pestes des petits ruminants virus (PPRV). Conversely, anti-HSV1 and anti-PPRV sera neutralized LV(CoV2 S) owing to the presence of CSP reactive antibodies indicating that a prior infection with such pathogens could impact on the pattern of COVID-19.

INTRODUCTION

The scale of infectivity and the spread of severe acute respiratory syndrome-coronavirus 2 (SARS-CoV2) that caused the COVID-19 pandemic continue to increase worldwide with the associated mortality now being in excess of five million (Hu et al., 2020). There has been unprecedented progress in developing vaccines and therapeutics against SARS-CoV2 and control of the pandemic seems to be a possibility despite the emergence of variants of concern (Jackson et al., 2020; Polack et al., 2020). The involvement of key immune mediators and the early signatures induced following vaccination that correlate with the success of vaccination are yet to be adequately reported. To further bolster the efforts against COVID-19, there is also a clear need for developing potent yet affordable therapeutics such as anti-viral monoclonal antibodies that can not only limit the consequences of COVID-19 but also be used to decipher events in the virus entry, intracellular trafficking as well as biogenesis of the virus. Many such steps could provide useful and much sought out anti-viral targets. Smaller variants of antibodies such as the fragment antigen binding (Fab), single chain fragment variable (scFv) or camelid sdAbs also referred to as nanobodies can also be used for potential therapy or prophylaxis (Dubey et al., 2020). Such sdAbs are well suited to neutralize infectious agents and toxins because of their ability to seek out cryptic epitopes that are usually inaccessible to the conventional antibodies as well as their inherent biophysical superior properties (Ingram et al., 2018; deMarco, 2011; Yu et al., 2020). Furthermore, we need to better understand how pre-existing antibodies induced against cross-reactive epitopes of heterologous infections might impact on the varied outcome of COVID-19 infection (Casadevall and Pirofski, 2020; Sehrawat and Rouse 2020).

The membrane anchored spike (S) protein of SARS-CoV2 facilitates entry in susceptible cells and therefore, has been a major target for anti-viral interventions (Huang et al., 2020; Salvatori et al., 2020). Proteases such as furin, and the host cell membrane associated TMPRSS2 process S protein by recognizing polybasic residues (RRAR) between S1/S2 and S2′sites generate S1, S2 and S2′ fragments. The cleaved fragments although remain non-covalently associated but alter the conformation of the S protein (Hoffmann et al., 2020; Peacock et al., 2021). This step is considered crucial for promoting the SARS-CoV2 infectivity (Jaimes et al., 2020; Winstone et al., 2021). We surmised that sdAbs against cleavage site (CS) encompassing peptide (CSP) of SARS-CoV2 S protein would represent a logical approach to pursue. Therefore, we selected sdAbs targeting the CSP as well as the RBD of SARS-CoV2 S protein from a camelid phage display library of variable region of heavy chain of heavy chain only antibody (V_HH) (Kaur et al., 2019). Characteristically, the sdAbs resisted structural and functional disruptions when exposed to harsh biophysical and biochemical conditions. Although both the antibodies neutralized a pseudovirus expressing surface SARS-CoV2 S

[1]Department of Biological Sciences, Indian Institute of Science Education and Research Mohali, Sector 81, SAS Nagar Knowledge City PO Manauli, Mohali, Punjab 140306, India

[2]These authors contributed equally

[3]Lead contact

*Correspondence: sharvan@iisermohali.ac.in

https://doi.org/10.1016/j.isci.2022.104549

protein LV(CoV2-S), anti-CSP sdAb when expressed as intrabody did so partly by interfering with the proteolytic cleavage of the S protein at the CSP and altering the fate of S protein making it inaccessible for the virion assembly. The anti-CSP sdAb neutralized *in vitro* and *in vivo* the infectivity of unrelated viruses such as herpes simplex virus 1 (HSV1) and a morbillivirus, i.e., pestis des petits ruminants virus (PPRV), both of which harbour polybasic sites in their entry mediators. These sites are RKRR in the glycoproteins B (gB) of HSV1 and RRTRR in the fusion (F) protein of PPRV. Furthermore, sera samples collected from the HSV1 or PPRV-infected animals neutralized the infectivity of LV(CoV2-S) whereas the sera samples depleted of CSP-specific antibodies failed to do so. These results suggested that such cross reactions might influence the pattern of responsiveness in COVID-19 patients.

RESULTS AND DISCUSSION

Selection and characterization of SARS-CoV2 specific sdAbs

We selected and characterized a sdAb against a peptide encompassing the polybasic CS (NSP**RRAR**/SVAS), interposed between S1/S2 fragments of the SARS-CoV2 S protein with the premise that such an antibody could compromise the proteolytic processing and reduce the virus infectivity (Figure S1s 1 and and Table 1). Furthermore, such antibodies might help decipher the virus biogenesis events. The purity and structural properties of the sdAbs were analysed by gel filtration chromatography, SDS-PAGE and circular dichroism (CD) (Figures 1A–1E and S1A,S1C, S1D). Fractions in peak 2 (P2) obtained using S200 columns contained a single band of fully folded anti-CSP sdAb as revealed by a prominent peak at 218nm and a minor peak at 230nm in the CD spectral plots (Figure S1D, inset). These spectral peaks indicated the presence of β sheets and exposed aromatic amino acids, respectively (Dumoulin et al., 2009). Dissociation constant (K_d) value for anti-CSP sdAb with SARS-CoV2 S proteins was 26nM (Figure 1B). The sdAb retained structural features between the pH range of 2–12 and remained stable when exposed to high temperature of 65°C (Figures 1C and 1D). Furthermore, the sdAb regained lost structure when the ambient temperature was gradually reduced (Figure 1E). Anti-CSP sdAb reacted with high ordered structures of the resolved CoV2 S protein as well as its monomeric form (~180kDa) whereas anti-FLAG mAb additionally recognized the polypeptide bands of ~130 and 95kDa in its FLAG-tagged version (Figures 1F and 1G). The data, therefore, suggested that anti-CSP sdAb recognized the unprocessed SARS-CoV2 S protein which could exist predominantly in a trimeric configuration. In addition, a sdAb against the receptor binding domain (RBD) of SARS-CoV2 S protein was selected from the phage display library using a predicted immunogenic epitope (YGFQPTNGVGYQ) as the bait and it was then characterized for immune reactivity, specificity and biophysical characteristics (Figures S1E–S1L). Similar to the results obtained for anti-CSP sdAb, the anti-RBD sdAb exhibited biophysical and biochemical robustness. Furthermore, such anti-RBD sdAb specifically recognised the cognate peptide and the recombinant RBD (Figure S1).

The immune reactivity and specificity of both the sdAbs were determined by western blotting and competitive ELISA against the index peptides, SARS-CoV2 S protein, recombinant RBD or pseudotyped lentivirus (LV) expressing SARS-CoV2 S protein. Anti-CSP sdAb when probed against the plate-bound selecting CSP or SARS-CoV2 S protein expectedly showed a concentration dependent increase in the OD_{405} values (Figures 1H and 1J). Anti-CSP sdAb when pre-incubated with the soluble CSP resulted in the reduced signal intensity against both the plate-coated CSP and SARS-CoV2 S that occurred in a concentration dependent manner (Figures 1I and 1K). These results attested to the specificity of anti-CSP sdAb. We then attempted to map the binding site of anti-CSP sdAb as this might provide insights into its potential anti-viral mechanisms. Trypsin, a serine protease that recognizes and cleaves basic residues, was incubated with the CSP in varying concentrations at either 37°C or 4°C and the mix was coated onto the wells in ELISA plates. Trypsin treated CSP at 37°C but not at 4°C showed reduced signal when probed with the anti-CSP sdAb, whereas the equivalent concentrations of a non-specific protein, BSA added to the CSP did not alter the assay readouts (Figures 1L–1O). Furthermore, a prior incubation of CSP with protease inhibitors followed by incubation with trypsin or the heat denatured trypsin yielded increasing OD_{405} values (Figures 1N and 1O). These results could mean that the anti-CSP sdAb recognized the epitope bordering S1/S2 segments in the SARS-CoV2 S protein that might have been erased by the proteolytic activity of trypsin. Data from these experiments could suggest that the anti-CSP sdAb, by masking the key residues in the CSP, prevented proteolysis of the CoV2 S protein. The cleavage of CoV2 S alters the presentation of the protein for enhanced infectivity.

Taken together, we selected SARS-CoV2 S protein specific sdAbs from a previously generated phage display library using synthetic peptides as the bait. We also established thermostability, specificity and

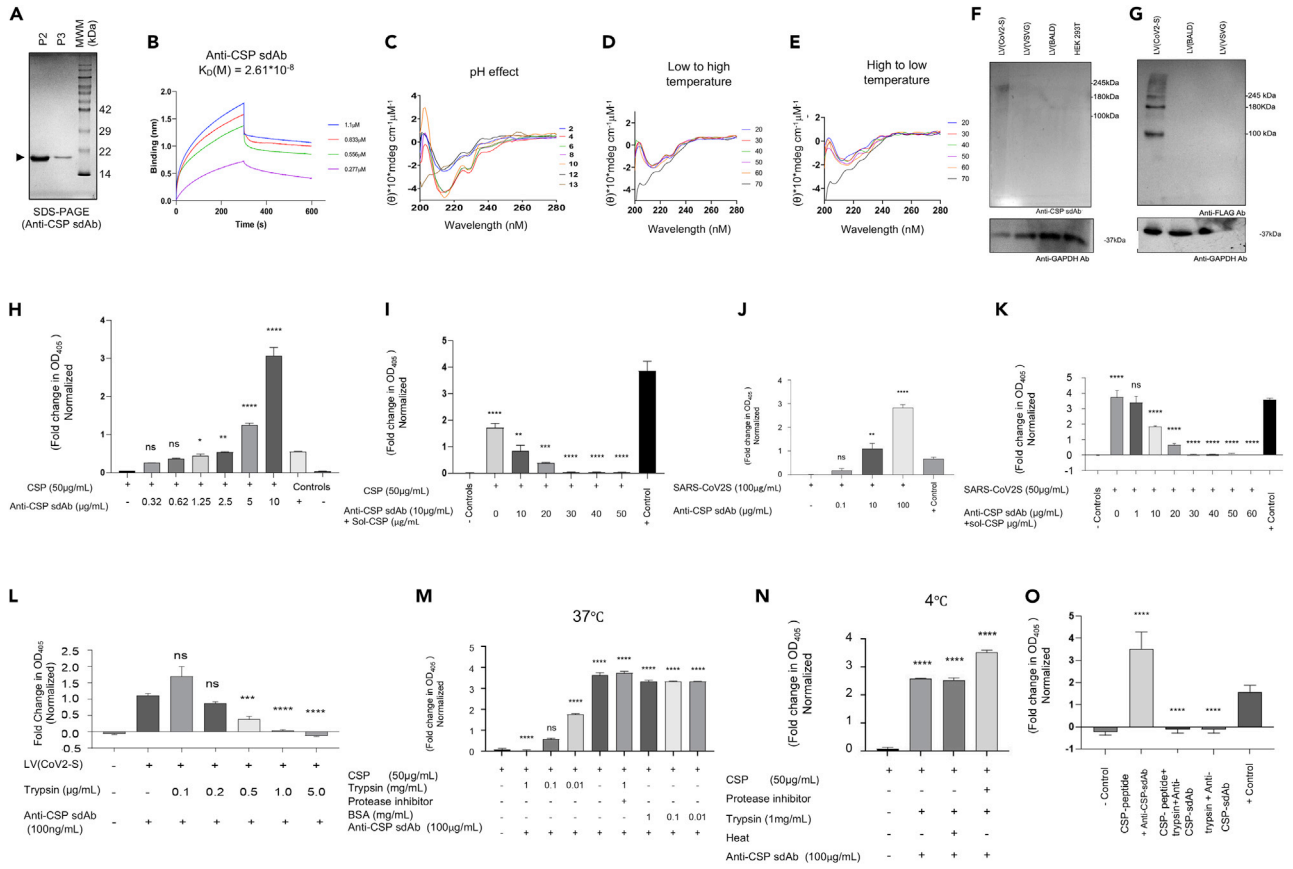

Figure 1. Selecting SARS-CoV2 specific sdAb by biopanning of phage display library

(A) SARS-CoV2 S specific sdAb against were selected from phage display library, subcloned, expressed and purified. A. The resolved peaks (P2 and P3) following S200 gel filtration chromatographic separation in a 12% reducing SDS-PAGE were stained with CBBR-250.

(B) The affinity of anti-CSP sdAb against the immobilised SARS-CoV2 S protein was determined by biolayer interferometry. The association and dissociation curve were used to measure the affinity of anti-CSP sdAb.

(C) The influence of varying pH on secondary structure of anti-CSP sdAb was measured using circular dichroism.

(D) The influence of an increasing temperature from 20°C to 70°C on the secondary structure of anti-CSP sdAb is shown by CD spectral analysis.

(E) The influence of decreasing the ambient temperature from 70°C to 20°C on the secondary structure of sdAb is shown by CD spectral analysis.

(F and G) The specificity of anti-CSP sdAb against the resolved recombinantly expressed S protein of SARS-CoV2 was analysed by immunoblotting. HEK293T cell lysates used for producing, LV (VSV-G), LV (BALD) and LV(CoV2-S) were resolved using a 12% reducing SDS-PAGE followed by western blotting with anti-CSP sdAb (F), anti-FLAG mAb (G). All experiments were repeated more than five times and representative images are shown.

(H–O)Determining the specificity and immune reactivity of anti-CSP sdAb.

(H) ELISA plates were coated with CSP (50 µg/mL) and probed using different concentrations of anti-CSP sdAb. Fold change in the mean OD_{405} values as compared to the mean OD_{405} values of negative controls is shown by bar diagram (as described earlier (Fagan et al., 2001)).

(I) ELISA plates were coated with CSP (50 µg/mL) and probed using anti-CSP sdAb pre-incubated with the indicated concentrations of its specific peptide and a fold change in the OD_{405} values as compared to mean OD_{405} values of negative controls is shown by bar diagram.

(J) ELISA plates were coated with SARS-CoV2 S (100 µg/mL) and probed with anti-CSP sdAb.

(K) Anti-CSP sdAb pre-incubated with different concentrations of soluble index peptide was used to probe immobilised SARS-CoV2 S protein and a fold change in the OD_{405} values in as compared to mean OD_{405} values of negative controls is shown by bar diagram.

(L) CSP was treated with different concentrations of trypsin at 37°C for three hours and the mix was coated onto ELISA plates. Anti-CSP sdAb was used for probing.

(M and N) CSP was treated with trypsin at 37°C (M) and 4°C (N) for three hours and the mix was coated onto ELISA plates. Anti-CSP sdAb was used for probing the treated CSP.

(O) CSP was treated with trypsin at 37°C for three hours and the mix was coated onto ELISA plates. Anti-CSP sdAb was used for probing. Positive controls were included where the antigen and its specific sdAb was used whereas multiple negative controls were included to ascertain the performance of the assay. The experiments were repeated four times with similar results. One-way ANOVA was used to measure the level of statistical significance. ****$p < 0.0001$, ***$p < 0.001$, *$p < 0.01$ and *$p < 0.05$. See also Figure S1.

immune reactivity of such antibodies not only against their selecting peptides but also against the SARS-CoV2 S protein and the RBD.

Anti-SARS-CoV2 sdAbs neutralize the virus infectivity and inhibit S protein mediated cell to cell fusion

We measured the neutralizing activity of both anti-CSP and anti-RBD sdAbs using a lentivirus (LV) based reporter pseudovirus system that expressed either SARS-CoV2 S or VSV-G proteins as the entry mediators (Figures 2A, S2A, and S3C). The scanning electron micrographs showed the presence of spikes on LV(CoV2-S) pseudovirus particles that were clearly absent in the control LV(VSV-G). Both the pseudovirues ranged 50 to 100nm in diameter (Figure S2A). The use of such pseudoviruses for analyzing the neutralizing activity can obviate the requirement of high containment facilities and the neutralization results are comparable to those obtained against the virulent virus *ex vivo* and *in vivo* (Garcia-Beltran et al., 2021; Zhao et al., 2013). Furthermore, such a system can efficiently be used for testing the neutralization of emerging mutants without necessarily culturing and isolating the variant. Vero E6 cells incubated with LV(CoV2-S) fluoresced within 24 h and the percent positivity increased up to 72 h after incubation. We obtained more than 70% GFP^{+ve} cells in different experiments. A prior incubation of LV(CoV2-S) with varying concentration of anti-CSP and or anti-RBD sdAb significantly reduced the cellular infectivity (Figures 2A, 2B, and 2E). Up to 50% neutralization efficiency was achieved at 100 ng/mL of anti-CSP sdAb and a near complete inhibition of the virus infectivity was observed at 5 μg/mL (Figures 2A, 2B, 2E, and S3C). The inhibitory concentration (IC_{50}) of anti-CSP sdAb was ~10 times lower than that of anti-RBD sdAb (Figure 2E). None of the sdAbs neutralized LV(VSV-G) even in ~10,000 M excess attesting to their functional specificity (Figures S2B–S2D). The heat denatured sdAbs regained structural features as the ambient temperature was reduced, we therefore tested whether such preparations could neutralize the virus (Figure 1E). Both the sdAb preparations neutralized the virus infectivity albeit with reduced efficiencies (Figures 2C–2E, S3D, and S3E). Anti-RBD sdAb interacted with the RBD of CoV2-S protein and in so doing seemingly inhibited RBD interaction with the ACE2. Thus, the increasing concentration of anti-RBD with pre-incubated M13 bacteriophages displaying RBD reduced the phage staining of Vero E6 cells (Our unpublished data). We then measured combinatorial effects of both the sdAbs in achieving the virus neutralization. We observed a slight improvement in neutralizing ability of both the sdAbs (each with 0.5 ng/mL) at lower concentration (Figures 2B and 2E, and S2F). Improved neutralization was recorded when a fixed sub-optimal concentration (5 ng/mL) of anti-CSP sdAb was combined with the varying concentrations of anti-RBD sdAb (Figures S2G and S2H). A further proof of the specificity of both the sdAbs was obtained by their pre-incubation with the cognate peptides and measuring the LV(CoV2-S) neutralization efficiency subsequently. Both the sdAbs exhibited reduced virus neutralization as the concentrations of the respective cognate peptides increased (Figures S2I–S2L,S3H, and S3I). These results demonstrated an efficient neutralization of a reporter pseudovirus expressing SARS-CoV2 S protein by the selected sdAbs.

SARS-CoV2 infects bystander cells by causing cell-to-cell fusion using the exposed S protein in the infected cells (Buchrieser et al., 2020). We, therefore, tested whether or not the sdAbs block such cell fusion events by interacting with the S protein. HEK293T cells used for generating pseudovirus that expressed CoV2-S ($HEK293T^{+LV(CoV2-S)}$) or the control particles ($HEK293T^{+LV(BALD)}$) were co-cultured with Vero E6 cells in the presence or absence of the sdAbs (Figures 3A–3C). Extensively diffused GFP staining was observed in the co-cultures of $HEK293T^{+LV(CoV2-S)}$ and Vero E6 cells suggesting for a heterologous fusogenic response (Figure 3A). A prior incubation of $HEK293T^{+LV\ (CoV2-S)}$ cells with either of the sdAbs but not with the control (anti-DNV sdAb) reduced the fusogenic activity by upto five-fold (Figures 3A–3C, S4, S5A–S5C, and S5E). Similarly, the sdAbs reduced the fusogenic activity by 4-fold when SARS-CoV2 S transfected HEK293T cells ($HEK293T^{+(CoV2-S)}$) were incubated with Vero E6 cells (Figures 3D–3F, S5A, S5B, S5D, and S5F). For such fusion events to occur, the viral S protein expression by the cells is a prerequisite (Buchrieser et al., 2020). We, therefore, measured the surface expression of S protein in HEK293T cells by flow cytometry using the biotinylated sdAbs and fluorescently labeled streptavidin (Figures 3G and 3H). Although the control cells ($HEK293^{+LV(BALD)}$) showed no staining with either of the sdAbs, the S protein surface expression was clearly evident in the transfected cells with S protein construct by both the sdAbs (Figures 3G and 3H). That both anti-CSP and anti-RBD sdAb detected surface expressed CoV2S suggested the abundance of intact and unprocessed surface displayed CoV2 S protein.

Taken together, we demonstrated that anti-SARS-CoV2 sdAbs blocked not only the virus entry in the susceptible cells but also prevented SARS-CoV2 S protein mediated fusogenic activity.

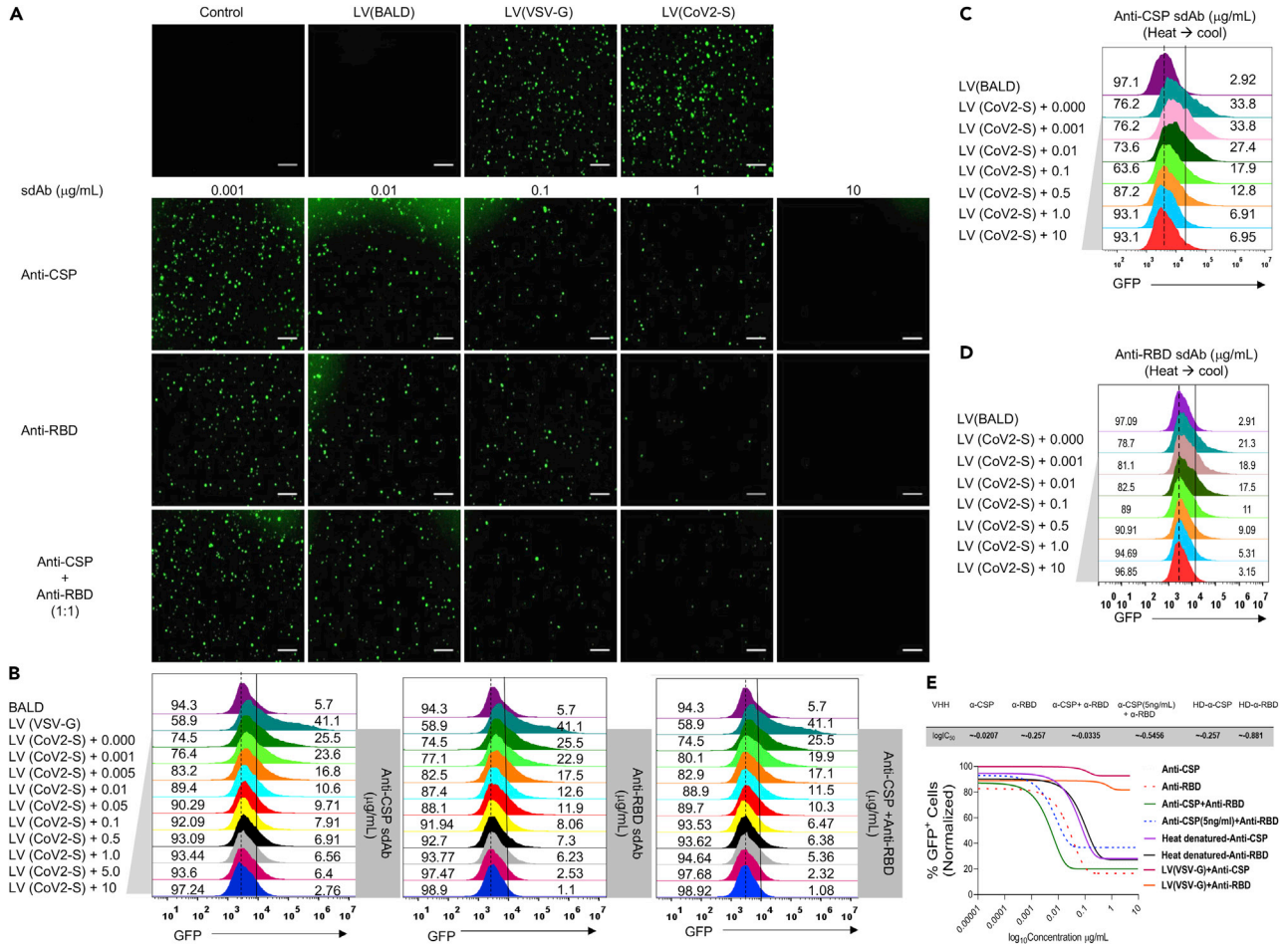

Figure 2. Anti-SARS-CoV2 S protein specific sdAb neutralize a reporter virus

The neutralizing potential of anti-SARS-CoV2 S protein specific sdAb was assessed using lentivirus (LV) based pseudovirus expressing SARS-CoV2 S, LV (CoV2-S) and VSV-G, LV (VSV-G). Vero E6 cells were infected with the pseudovirus particles alone or the pseudovirus particles pre-incubated with anti-CSP and/or anti-RBD sdAb at 4°C. Green fluorescence emitted by such cells was analysed by fluorescent microscopy and flow cytometry.

(A) Representative fluorescent microscopic images show the extent of neutralization of LV (CoV2-S) by different concentrations of anti-CSP and/or anti-RBD sdAb. For measuring the combinatorial effect the sdAb, one-half of the doses were similarly used. Scale bar is 160μm.

(B) Representative offset histograms obtained by flow cytometric analysis show GFP^{+ve} cells infected with LV(CoV2-S) or the anti-CSP and/anti-RBD sdAb neutralized LV (CoV2-S) in indicated conditions.

(C) Representative offset histograms obtained by flow cytometry show GFP^{+ve} cells infected with native LV (CoV2-S) or those pre-incubated with the high temperature exposed anti-CSP sdAb followed by its cooling at room temperature LV (CoV2-S).

(D) Representative offset histograms obtained by flow cytometry show GFP^{+ve} cells infected with native LV (CoV2-S) or those pre-incubated with the high temperature exposed anti-RBD sdAb followed by its cooling at room temperature LV (CoV2-S). Vertical dotted line serves as the reference for marking the peak and vertical dark lines represents the marker to separate GFP^{+ve} and GFP^{-ve} cells.

(E) Cumulative data obtained from the neutralization experiments (A–D) along with the inhibitory concentrations are depicted. The experiments were performed for at least five times with similar results. One-way ANOVA was used to measure the level of statistical significance. ****$p < 0.0001$, ***$p < 0.001$, *$p < 0.01$ and *$p < 0.05$. See also Figures S2, S3, S4.

Anti-CSP sdAb inhibits SARS-CoV2 infectivity by preventing proteolytic cleavage of the viral S protein

It is considered that the proteolytic processing of SARS-CoV2 S protein is critical for the virus infectivity. We, therefore, compared the immunological reactivity of anti-CSP sdAb against LV(CoV2-S) and pseudovirus expressing a mutant cleavage site, LV(CoV2-S, mut CS). Anti-CSP sdAb did not react with the lysates of HEK293T cells used for generating the mutant virus, $HEK293T^{+(CoV2S,\ mut\ S)}$, whereas polypeptide bands of ~180kDa and high MW were observed in the cell lysates used for generating the pseudovirus expressing WT SARS-COV2 S protein ($HEK293T^{+(CoV2S)}$) (Figure 4A). Furthermore, LV(CoV2-S, mut CS) did not

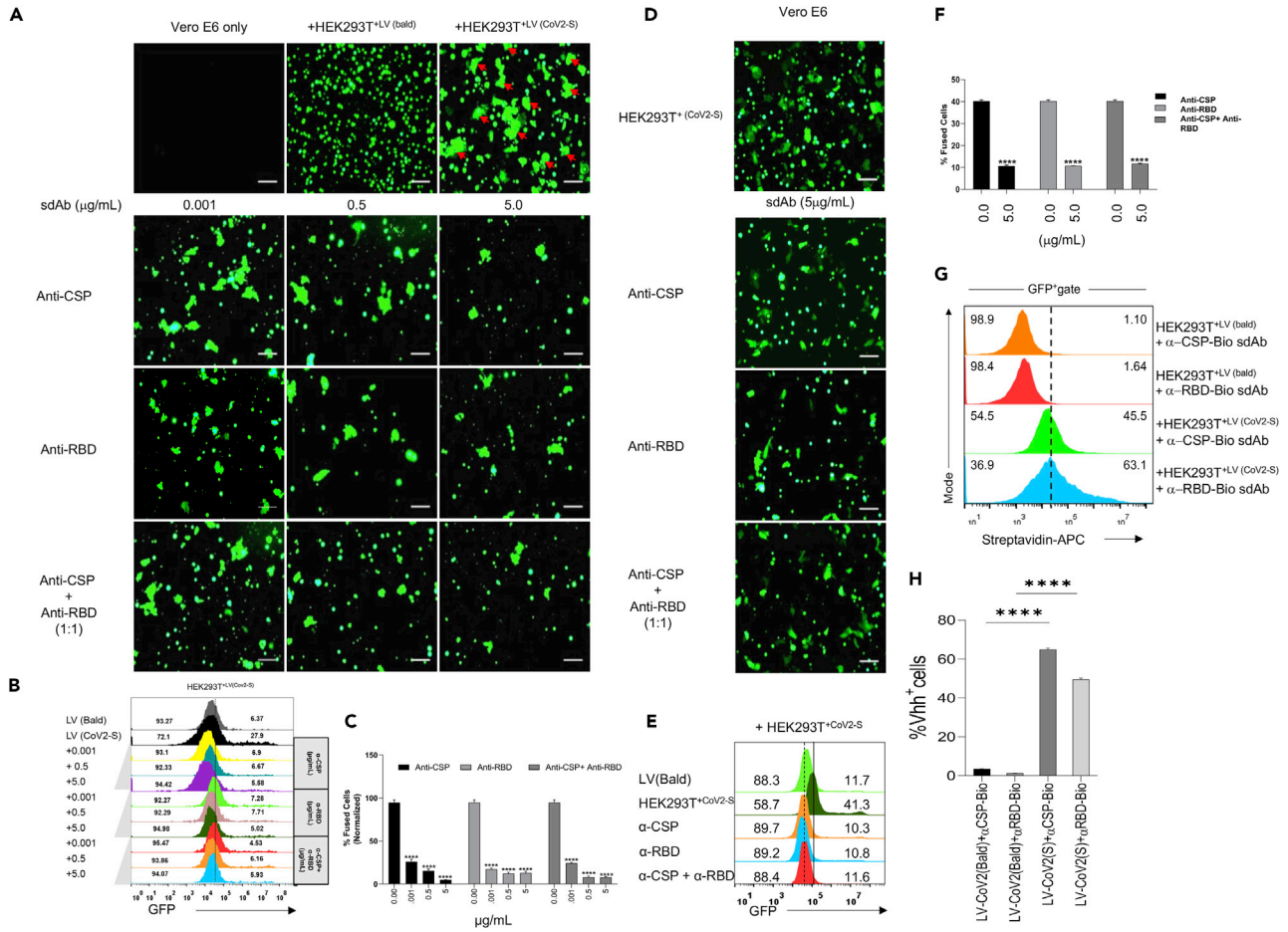

Figure 3. Anti-SARS-CoV2 S protein sdAbs inhibit cell to cell fusion

HEK293T cells used for producing LV(CoV2-S); HEK293T$^{+LV(CoV2\text{-}S)}$ and LV(BALD); HEK293T$^{+LV(BALD)}$ were co-cultured with Vero E6 cells in the presence or absence of anti-CSP and/or anti-RBD sdAb and the percentages of fused cells were analysed by fluorescent microscopy and flow cytometry.

(A) Representative fluorescent images from the indicated conditions are shown. Red arrow heads indicate fused cells (diffused GFP staining) in the co-culture of Vero E6 cells and HEK293T$^{+LV(CoV2\text{-}S)}$ cells whereas no such staining pattern was observed in the co-culture of Vero E6 cells and HEK293T$^{+LV(BALD)}$ cells. The extent of fused cells is shown when HEK293T$^{+LV\ (CoV2\text{-}S)}$ cells were pre-incubated with anti-CSP and/or anti-RBD sdAb when used alone or in combination at indicated concentrations. Scale bar is 160μm.

(B) Representative offset histograms show the percentage of fused cells in different conditions. Gating strategy for determining the percentage of fused cells is shown in Figure S3.

(C) Bar diagrams show the normalized proportion of fused cells in the co-culture with or without different concentrations of anti-CSP or/and anti-RBD sdAb. The levels of statistical significance were measured by two way ANOVA. ****p < 0.0001, ***p <0.001, *p < 0.01 and *p < 0.05.

(D) The fusogenic response of HEK293T cells transfected with SARS-CoV2 S construct, HEK293T$^{(CoV2\text{-}S)}$ when cultured with Vero E6 cells in the presence or absence of anti-CSP and/or anti-RBD sdAb is shown by fluorescent images. Scale bar is 160μm.

(E) Representative histograms show the percentage of fused cells in different conditions. Vertical dark line represents the marker to separate GFP^{+ve} and GFP^{-ve} cells shown in percentages. Gating strategy for determining the percent fused cells is shown in Figure S3.

(F) Bar diagrams depict the percentage of fused cells in co-culture with or without different concentrations of anti-CSP or/and anti-RBD sdAb. The levels of statistical significance were measured by two way ANOVA. ****p < 0.0001, ***p <0.001, *p < 0.01 and *p < 0.05.

(G) Surface expression of SARS-CoV2 S protein by HEK293T$^{+LV(CoV2\text{-}S)}$ was measured by flow cytometry using biotinylated anti-CSP and anti-RBD sdAb and representative histograms show percent positive cells.

(H) Bar diagram show the percentage positive cells within different conditions. The experiments were repeated five times with similar results. The levels of statistical significance were measured by one-way ANOVA. ****p < 0.0001, ***p < 0.001, *p < 0.01 and *p < 0.05. See also Figures S3, S4 and S5.

demonstrate reactivity with anti-CSP sdAb whereas the anti-RBD sdAb detected it in a dose-dependent manner (Figure 4B). These results might indicate that LV(CoV2-S, mut CS) particles might have been decorated with the unprocessed S protein which were not recognised by the anti-CSP sdAb. We then compared in a head-to-head fashion the internalization of LV(CoV2-S) and LV(CoV2-S, mut CS) in Vero E6 cells using

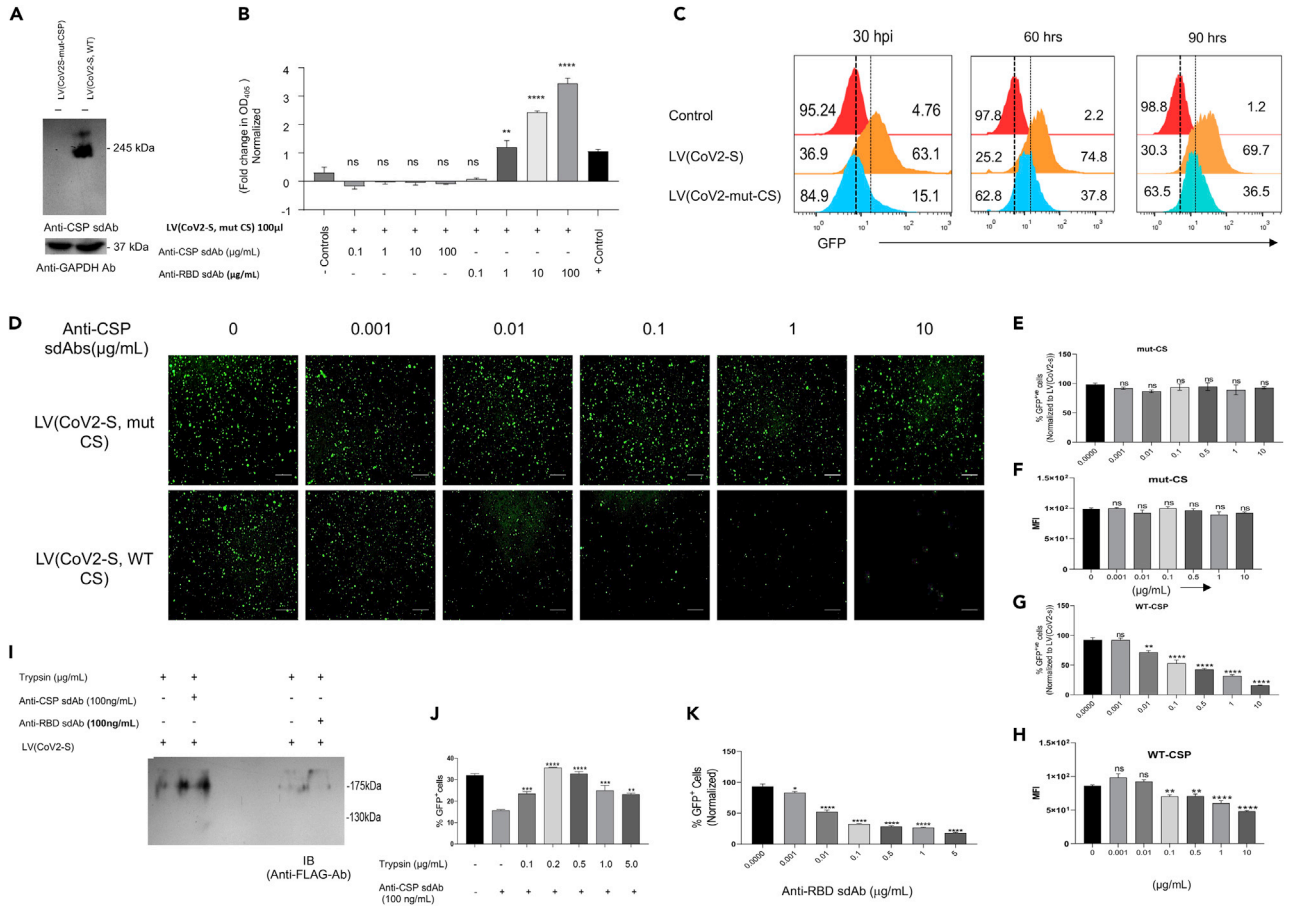

Figure 4. Anti-CSP sdAb exhibit anti-viral mechanisms by interfering with the proteolytic processing of S protein

Pseudovirus particles expressing WT and CS mutant S protein SARS-CoV2 S protein viz., LV(CoV2-S) and LV(CoV2-S, mut CS),respectively.

(A) The lysates from HEK293T$^{+LV(CoV2\text{-}S)}$ and HEK293T$^{+LV(CoV2\text{-}S,\ mut\ CS)}$ were resolved using a 12% SDS-PAGE and the transferred polypeptides were probed with anti-CSP sdAb and anti-GAPDH mAb.

(B) ELISA plates were coated with LV(CoV2-S, mut CS) and probed with anti-CSP or anti-RBD sdAb. Fold change in the mean OD_{405} values are shown by bar diagrams.

(C) Equal concentrations of LV(CoV2-S) and LV(CoV2-S, mut CS) were used to infect Vero E6 cells and the extent of infectivity was measured at different time points by flow cytometry using GFP^{+ve} cells. Representative offset histograms from indicated conditions were used to determine GFP^{+ve} cells. Vertical dark line represents the marker to separate GFP^{+ve} and GFP^{-ve} cells shown in percentages.

(D–F) Anti-CSP sdAb were assessed for neutralizing the infectivity of LV(CoV2-S) and a high concentration of LV(CoV2-S, mut CS) using Vero E6 cells.

(D) Representative fluorescent images from the indicated conditions are shown. Scale bar is 160 µm.

(E and F) Bar diagrams show the normalized proportion of GFP^{+ve} cells (E) and MFI (F) measured by flow cytometry with or without different concentrations of anti-CSP sdAb for LV(CoV2-S, mut CS).

(G and H) Bar diagrams show the normalized proportion of GFP^{+ve} cells (G) and MFI (H) measured by flow cytometry with or without different concentrations of anti-CSP sdAb for LV(CoV2-S).

(I) Anti-CSP or anti-RBD sdAb was incubated with LV(CoV2-S) and the mix was then treated with trypsin. The treated particles were then analysed by western blotting using anti-FLAG mAb. J. Trypsinised LV(CoV2-S) were used to infect Vero E6 cells. Bar diagram shows the frequencies of GFP^{+ve} cells.

(K) Anti-RBD sdAb was incubated with trypsinised LV(CoV2-S) and the pseudoviruses were then used to infect Vero E6 cells. The infectivity was measured by fluorescence microscopy and flow cytometry. Bar diagram shows the frequencies of GFP^{+ve} cells. The experiments were repeated three times and similar results were obtained. The levels of statistical significance were measured by one-way ANOVA. ****$p < 0.0001$, ***$p < 0.001$, *$p < 0.01$ and *$p < 0.05$. See also Figures S3, S6, and S7.

equal content of both the pseudoviruses (Figure S6A). We observed up to a four-fold reduction in the frequencies of GFP^{+ve} Vero E6 cells with LV(CoV2-S, mut CS) as compared to those infected with WT LV(CoV2-S) at 30hpi (Figures 4C, S6B, andS3A). At later time points, such differences were up to two-fold indicating that the proteolytic cleavage of S protein to yield S1 and S2 subunits could serve as a critical initial event in facilitating the virus infectivity (Figures 4C and S6B). Enhanced infectivity of the mutant virus

at a later time might have been attributed to the cleavage of S protein downstream to the canonical polybasic site that conceivably represented a less favoured step in facilitating the virus entry. It was recently shown that the absence of furin cleavage site (PRRAR) reduced the processing of S0 by approximately 15% (Johnson et al., 2021). Therefore, the absence of such a furin cleavage site might not completely abolish the processing of S protein which could be compensated by the involvement of downstream sites for such events to occur. The mutated polybasic site nonetheless slowed the kinetics of infection in addition to reducing the overall infectivity (Papa et al., 2021). We then used a up to 10 fold higher concentration of LV(CoV2-S, mut CS) to assess if anti-CSP sdAb could block the virus infectivity independent of its binding to the polybasic CS in S protein (Figures 4D–4F). Anti-CSP sdAb inhibited WT LV(CoV2-S) infectivity in a dose dependent manner but not that of LV(CoV2-S, mut CS) (Figures 4D–4H). We then tested whether or not anti-CSP sdAb inhibited the trypsin-mediated cleavage of the S protein. A prior incubation of LV(CoV2-S) with anti-CSP sdAb but not with anti-RBD sdAb prevented the proteolysis of S protein as a polypeptide band of ~180kDa was observed in the latter case (Figure 4I) (Johnson et al., 2021). Furthermore, the plate-coated LV(CoV2-S) but not the trypsinized LV(CoV2-S) particles reacted with anti-CSP sdAb in ELISA (Figure 1L and S6C). These results showed that anti-CSP sdAb blocked SARS-CoV2 infectivity by recognizing the unprocessed S protein (S0) displaying LV(CoV2-S) and prevented its proteolytic processing to inhibit the internalization process. Although the trypsin treatment rendered LV(CoV2-S) refractory to neutralization by anti-CSP sdAb, the graded concentrations of anti-RBD sdAb efficiently blocked its internalization (Figures 4J, 4K, S6D, S6E, S3F, and S3G). That the prior incubation of LV(CoV2-S) with either of the sdAbs followed by trypsin treatment significantly inhibited the internalization process suggested for their recognition of distinct sites in the S protein (Figures S6F and S6G). Furthermore, the culture supernatants of Vero E6 cells incubated with the equal concentration of LV(CoV2-S) alone or those added with the anti-CSP sdAb showed an increasing concentration of the unprocessed viral S protein suggesting for less efficient LV(CoV2-S) internalization (Figure S6H).

These results showed that the anti-CSP sdAb blocked infectivity of LV(CoV2-S) by recognizing the unprocessed S protein (S0) displayed by LV(CoV2-S) and prevented its proteolytic processing that served as an infection enhancing factor.

Anti-SARS-CoV2 S protein intrabodies inhibit viral assembly and biogenesis

The biogenesis and assembly of SARS-CoV2 virions in the infected cells require synthesis of viral proteins followed by transport via trans-Golgi network (deBreyne et al., 2020; V'kovski et al., 2020). However, many such events remain less defined. We investigated whether or not anti-SARS-CoV2 S specific sdAbs when expressed intracellularly engage with the newly synthesised S protein given their specificity towards linear epitopes. Could such intracellular interactions hamper the biogenesis of pseudovirions expressing the S protein? The anti-CSP intrabody by binding to the CSP of the newly synthesised S protein could either make the cleavage site inaccessible to proteolytic processing and consequently its compromised incorporation in the newly formed virions. This could also preferentially target the S protein for degradation. We cloned both anti-CSP and anti-RBD sdAbs separately in pLenti-GFP vector and expressed as fusion products with GFP in HEK293T cells (Figure 5A). The translated products expectedly showed 42kDa polypeptide bands in the lysates of transfected HEK293T cells probed using an anti-Myc tag Ab, whereas no such bands were observed in the control pLenti-GFP vector transfected cells (Figure S7G). In order to analyse the representation of different fragments of CoV2S protein, the lysates from transfected control cells, tunicamycin treated and the anti-CSP IB expressing groups were probed with anti-6x(HIS) Ab. We observed that the control cells at 72h post transfection had lesser content of the S protein in comparison to those from the other groups which could be because of inefficient utilization in the assembly of CoV2 S expressing pseudovirions (Figure 5B). As compared to the control transfected cells, tunicamycin treated and the anti-CSP IB expressing cells showed prominent polypeptide bands of the S protein in the lower molecular weight range which might suggest an enhanced degradation. Tunicamycin, an antibiotic that helps retain newly synthesized proteins in the ER and in so doing alters post translational modification such as N-linked glycosylation occurring in Golgi complexes. This step inhibits the formation of pseudoviruses from the transfected HEK293 T cells (Rottier et al., 1981). When analysed for the presence of surface CoV2 S protein by ELISA, the collected pseudovirions revealed an enhanced expression in the control cells in comparison to the other two groups indicating the compromised synthesis of LV(CoV2-S) in tunicamycin treated and the anti-CSP IB expressing cells (Figure 5C). We also measured the content of pseudovirions produced from control, tunicamycin and the anti-CSP IB expressing cells using both the biotinylated anti-RBD and anti-CSP sdAbs and observed a reduced signal by both the antibodies (Figures S7C and S7D).

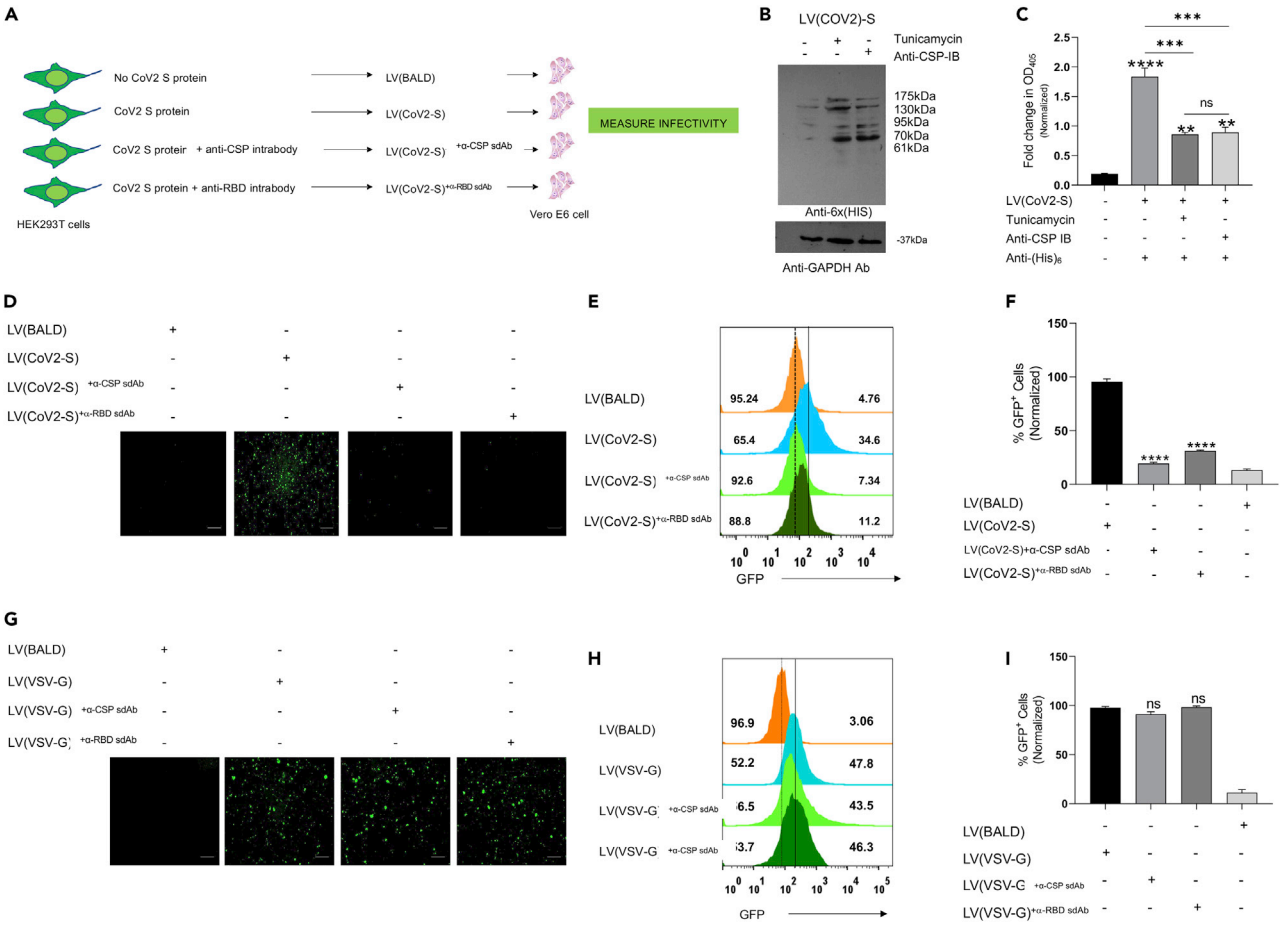

Figure 5. Anti-SARS CoV2 S specific intrabodies inhibit the production of pseudovirions expressing the S protein

(A) A schematic for measuring the influence of intrabodies in pseudovirions production that express S protein. HEK293T cells were transfected with plasmids encoding for the anti-CSP and anti-RBD sdAb in frame with GFP in the pLentiGFP vector to express the sdAb intracellularly. The pseudovirus particles produced were concentrated and used to infect Vero E6 cells. The cells were analysed by fluorescence microscopy and flow cytometry.

(B)Western blot from the lysates of HEK293T cells, which were used to generate LV(CoV2-S) pseudoviruses either in presence of Tunicamycin (2 μg/mL) or in the presence of anti-CSP intrabodies, showing different banding pattern of the S protein and loading control (GAPDH).

(C) ELISA plates were coated with supernatants generated from above setup and probed using Anti-$(HIS)_6$ antibody. Fold change in the mean OD_{405} values as compared to the mean OD_{405} values of negative controls is shown by bar diagram. The experiments were repeated three times with similar results. One-way ANOVA was used to measure the level of statistical significance. ****$p < 0.0001$, ***$p < 0.001$, *$p < 0.01$ and *$p < 0.05$.

(D) Representative fluorescence micrographs from the indicated conditions are shown. Scale bar is 160 μm.

(E) Offset histograms show GFP^{+ve} cells in different conditions. Vertical dark line represents the marker to separate GFP^{+ve} and GFP^{-ve} cells shown in percentages.

(F) Bar diagrams show the normalized percentages of GFP^{+ve} cells in indicated conditions.

(G) Representative fluorescence micrographs from the indicated conditions are shown where S construct was replaced with VSV-G expressing construct for control experiments. Scale bar is 160 μm.

(H) Offset histograms show GFP^{+ve} cells in different conditions where LV(VSV-G) based pseudoviruses were used to transduce Vero E6 cells.

(I) Bar diagrams showing the normalized percentages of GFP^{+ve} cells in indicated conditions. The experiments were repeated three times and similar results were obtained. The levels of statistical significance were measured by one-way ANOVA. ****$p < 0.0001$, ***$p < 0.001$, *$p < 0.01$ and *$p < 0.05$. See also Figures S3 and S7.

Deglycosylation of the pseudoviruses obtained from the control cells resulted in reduced signal by the anti-CSP sdAb only which might suggest that carbohydrate moieties might or the presentation of amino acid residues could result in an efficient recognition by anti-CSP sdAb. The produced LV(CoV2-S) particles collected from the supernatant of HEK293 T cells were used to infect Vero E6 cells. We observed ~90% reduced frequency of GFP^{+ve} Vero E6 cells infected with LV (CoV2-S) from HEK293T cells expressing the anti-CoV2 S specific IB in comparison to those infected with pseudoviruses obtained from control cells at 72hpi (Figures 5D–5F). The cells expressing IB were not generically compromised in the biosynthesis

of pseudoviruses as LV(VSV-G) produced by such cells equipotently infected Vero E6 cells (Figures 5G–5I and S3K). To further investigate possible mechanisms by which anti-CSP IB exhibited anti-viral functions, we analysed surface and intracellular expression of the CoV2 S protein in the transfected cells that were subjected to different treatment conditions. As compared to the control cells, tunicamycin treated cells or those expressing anti-CSP IB had reduced surface expression of CoV2 S protein. The exposure of such cells with a proteasomal inhibitor, MG132, enhanced intracellular expression of CoV2 S in both tunicamycin treated and the anti-CSP IB expressing cells (Figures S7A, S7B, and S3B). These results indicated that anti-CSP IB could facilitate proteolytic degradation of newly synthesized CoV2 S protein. Whether or not the anti-CSP IB efficiently targeted CoV2 S protein for degradation was analysed by measuring the ubiquitination status of the purified CoV2 S protein from control, tunicamycin and the anti-CSP IB expressing cells. We observed distinct polypeptide bands and more species of Ni-NTA purified CoV2 S protein resolved in lower molecular mass range that were recognized by anti-Ub Ab in the anti-CSP IB expressing cells in comparison to the control cells (Figure S7H, upper panel). Furthermore, Ni-NTA beads precipitated CoV2 S protein with the anti-CSP IB as measured by anti-Myc Ab (Figure S7H, middle panel). To analyse the localization of anti-CSP IB and the CoV2 S protein, we performed confocal microscopy. Control cells not transfected with the anti-CSP IB showed diffused CoV2 S protein expression predominantly localizing with calnexin, an ER marker and Golgin, Golgi marker (Figures S7I–S7J). In both tunicamycin treated cells and the anti-CSP IB expressing cells, we observed a focal staining of the CoV2 S protein surrounding the nucleus (Figures S7I–S7J). The localization of anti-CSP IB marked by GFP and the CoV2 S protein was predominantly observed at an early time point at 24 hour post transfection (Figure S7I). These results not only demonstrated the co-localization of CoV2 S protein with anti-CSP IB but also the anti-CSP IB mediated degradation led to low expression levels.

Taken together we established not only the intracellular specificity of the anti-SARS-CoV2 IB but also their potential to reduce LV-CoV2 S pseudovirions production.

Anti-CSP sdAb neutralizes unrelated viruses with cross reactive polybasic CS surface proteins

Largely conserved CSPs serve as virulence factor for many microbes or their products (Braun and Sauter, 2019; Izaguirre, 2019). The preponderance of proteolytic enzymes at tissue sites or those induced following infection promote the infectivity by processing such CSPs (Braun and Sauter, 2019; Izaguirre, 2019). The entry mediators could be re-configured by proteolytic events to facilitate the fusion of virions with the cellular membrane and subsequent internalization events. Some viruses with their protein products as well as the sequences contained in their respective CSPs are shown in Figure S8A. To provide a proof-of-principle evidence that such sites are immunogenic and that the anti-CSP sdAb recognizes such sites, we measured whether or not anti-CSP sdAb could neutralize two such viruses *viz.*, HSV1 and PPRV. HSV1 is a ubiquitously prevalent virus infection of humans and PPRV is a morbillivirus, the other member of the genus being measles virus that infects children. We observed up to a 100-fold reduction in the viral titer using plaque assays when either of the viruses were separately pre-incubated with anti-CSP sdAb followed by infecting Vero cells (Figures 6A and S8B). We also measured the influence of anti-CSP sdAb on HSV1 neutralization *in vivo* by infecting RAG1$^{-/-}$ mice. This model was used for assessing the pathogenicity of HSV1 (Ramakrishna et al., 2015). We observed a significantly high mortality in the infected controls as compared to the animals infected with anti-CSP sdAb neutralized HSV1 (Figure 6B). All infected controls succumbed to the virus infection within 15dpi but the animals in anti-CSP sdAb group survived. Furthermore, animals receiving HSV1 or the neutralized virus were followed over time for measuring their change in body weights. Although the animals injected with anti-CSP sdAb neutralized HSV1 only transiently reduced their body weights, those injected with HSV1 gradually lost body weights for the entire observation period until 15dpi (Figure 6C). Similarly, IFNR$^{-/-}$ mice injected with the anti-CSP sdAb neutralized PPRV reduced body weights to a lesser extent as compared to those injected with equivalent doses of un-neutralized PPRV when tested in a recently described model (Figure S8C, (Sharma et al., 2021). To measure the virus neutralization by anti-CSP sdAb, separate groups of animals infected with HSV1 or the anti-CSP sdAb neutralized HSV1 were sacrificed on 10dpi to assess the viral load in different organs. The animals in the HSV1 only group showed a greater reduction in body weights as compared to those in the anti-CSP sdAb neutralized HSV1 group (Figure S9A). No replicating virus particles were detected in lungs, liver and kidneys of animal from any of the groups (data not shown). However, the replicating HSV1 particles were recovered from brain tissues of the HSV1 injected animals but not from those in the anti-CSP sdAb neutralized HSV1 group (Figure S9B). These results demonstrated the neutralizing ability of anti-CSP

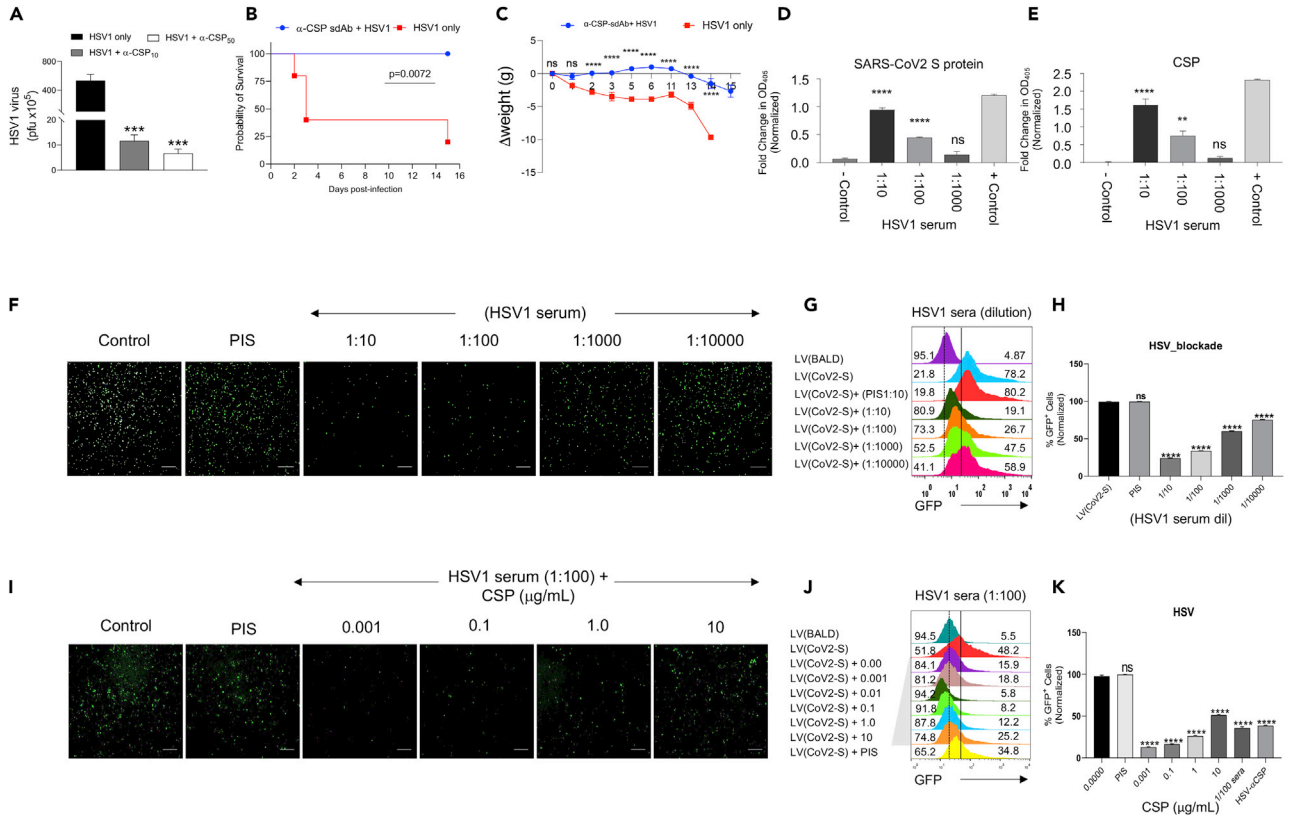

Figure 6. Anti-polybasic cleavage site sdAb or those induced by such sites carrying heterologous virus infections neutralize SARS-CoV2

(A) HSV1 incubated with 10 and 50 μg/mL of anti-CSP sdAb or the native HSV1 were compared for their infectivity using Vero cells by plaque forming assays. Bar diagrams show viral titers in each group.

(B and C) For measuring the neutralization of HSV1 by anti-CSP sdAb, RAG1$^{-/-}$ mice were divided into two groups. Animals in one group were intraperitoneally infected with 5 × 10^5 pfu of HSV1 pre-incubated with 50μg of anti-CSP sdAb whereas the other groups received only 5 × 10^5 pfu of the virus. The animals were analysed for induced mortality and weight loss over the course of infection.

(B) Survival plot summarizes the mortality of animals in each group (n = 6; Log-rank (Mantel-Cox) test).

(C) Plots show the change in body weights of animals in the indicated group. The experiments were repeated three times with similar results.

(D and E) Cross-reactivity of anti-HSV1 serum with SARS-CoV2-S protein was determined by ELISA. Cumulative bar diagrams show the OD_{405} values obtained after probing the coated SARS-CoV2 S protein (D) and CSP (E) with different dilutions of the anti-HSV1 sera samples by ELISA.

(F–H) A cellular assay to assess the cross neutralization of LV(CoV2-S) by anti-HSV1 serum was performed. Indicated dilutions of the anti-serum were pre-incubated with LV(CoV2-S). The pre-incubated LV(CoV2-S) was then used to infect Vero E6 cells and the extent of infectivity was measured by anti-HSV1 or preimmune serum. Representative images (F) show the distribution of green fluorescence 72 h after infection with untreated (Control), pre-immune serum treated (PIS) and HSV1 serum treated LV(CoV2-S). Scale bar is 160μm.

(G) Representative histogram plots show percent infected cells in different conditions.

(H) Bar diagrams show the cumulative data from a representative experiment shown in F and G.

(I–K) Different concentrations of CSPs were added to 1:100 diluted anti-HSV1 sera to deplete polybasic site specific antibodies which was then used for incubating with LV(CoV2-S). The pre-incubated LV(CoV2-S) particles were then added to Vero E6 cells for measuring the infectivity. Representative micrographs (I) and histogram plots (J) show GFP^{+ve} cells after 72 h of incubation.Scale bars in micrographs is 160μm.

(K) Bar diagrams summarize the data from one such experiments. The experiments were repeated three times and the levels of statistical significance were measured by one-way ANOVA. ****p < 0.0001, ***p < 0.001, *p < 0.01 and *p < 0.05. See also Figure S8 and S9.

sdAb *in vitro* as well as *in vivo* against unrelated viruses sharing largely conserved polybasic sites in their entry mediators with the SARS-CoV2 S protein.

In order to assess the physiological relevance of polybasic sites occurring in viruses in inducing antibodies in the infected animals, we measured whether or not the antibodies induced against HSV1 or PPRV cross-reacted with the CSP. Sera samples from HSV1 or PPRV infected animals but not from uninfected controls reacted with immobilized CSP as well as the SARS-CoV2 S protein at dilution of 1:100 in ELISA (Figures 6D, 6E, S8D, and S8E). Moreover, anti-HSV1 and anti-PPRV sera neutralized the LV(CoV2-S) by ~50% levels up

Table 1. Primers used for cloning of Intrabodies into pLenti-GFP and in YBNT vectors for protein expression

Primer Name	Primer sequences
FP VHH FR1 pLenti	5′-GCATTCTAGAGGCACCCCGGGA TGGCCGATGTTCAACTGCAGGAG-3′
FR4 C-Mvc pLenti	5′-GCTAGGATCCTGCAGATCC TCTTCAGAGATGAGTTTCTGC TCTGTGGAGACGGTGACCTG-3′
MKS-9 (VHH FP)	5′-GTTGTGTGGAATTGTGAGCG-3′
MKS-22 (VHH RP)	5′-GAAATGCGGCCGCTGTGGA GACGGTGACCTG-3′
T7-EP	5′-TAATACGACTCACTATAGGGG AATTGTG-3′
T7-RP	5′-GCTAGTTATTGCTCAGCGGTG GCAGCAGC-3′

to a 1: 1,000 and 1:800 dilution, respectively. We also observed a significant neutralization even at 1:10,000 dilution by both the sera samples (Figures 6F–6H, S8F–S8H, S9F, and S9G). The sera samples at 1:10 dilution from uninfected animals failed to neutralize the pseudovirus particles (Figures 6F–6H, S8F, S8H, and S9F, G). Whether or not CSP adsorbed anti-HSV1 and PPRV sera samples were compromised in neutralizing LV(CoV2-S) was assessed by incubating them with plate bound CSP. The efficiency of neutralization of LV(CoV2-S) was significantly reduced by both anti-HSV1 and PPRV sera with the increasing concentrations of pre-incubated CSP (Figures 6I–6K). Accordingly, we observed ~50% reduction in the LV(CoV2-S) neutralization by anti-HSV1 sera with the addition of 10μg of CSP whereas 1μg of CSP achieved similar level of reduction for anti-PPRV sera (Figures 6I–6K, S8I–S8K). The magnitude or the quality of cross-reactive antibodies induced against the CSP in HSV1 and PPRV infected animals could account for the observed variations in neutralization efficiencies. Thus, HSV1 sera samples were collected from infected WT animals whereas PPRV sera samples were collected from infected $IFNR^{-/-}$ mice. Signalling via IFNR influences the magnitude and quantity of induced antibody response has been demonstrated previously (Lee et al., 2020; Swanson et al., 2010). We also measured the neutralizing efficiency of anti-HSV1 or anti-PPRV sera samples or those adsorbed with CSP against both the viruses using plaque assays. The increasing concentrations of CSP added to the respective sera samples reduced the neutralizing ability in a dose dependent fashion against both HSV1 and PPRV (Figures S9C and S9D). These results clearly demonstrated that anti-CSP specific antibodies were induced following HSV1 and PPRV infections and such antibodies neutralized homologous as well as completely unrelated virus, LV(CoV2-S), because of their shared epitopes in the exposed proteins carrying the polybasic residues.

That the antibodies from HSV1 infected animals cross-neutralized LV(CoV2-S) raised the question whether or not HSV1 seropositive individuals could better control SARS-CoV2 as compared to seronegative individuals. No immunological or epidemiological data is available favouring or opposing the notion. However, our meta-analysis aimed at comparing the case load and mortality of COVID-19 with the prevalence of HSV1 infection indicated for a reverse trend in different regions of world (Figure S9E). Although inherent caveats in data collection and reporting of all infection need to be factored in, there seems to be a negative correlation between HSV1 seropositivity and COVID-19 cases.

The uniquely acquired CSPs by SARS-CoV2 is proposed as a virulent factor to enhance infectivity (Qiao and DeLa Cruz, 2020). Not only SARS-CoV2 but many other viruses such as herpesviruses and the members of paramyxoviridae, bacterial products and toxins enhance their pathogenicity and toxicity by such acquisitions and adaptations (Braun and Sauter, 2019; Izaguirre, 2019; Schrauwen et al., 2012). Therefore, it is conceivable that targeting such sites could be considered as a broad-based neutralization strategy against multiple pathogens. The proteolytic enzymes are abundantly present at infected tissue sites as well as in the membrane of susceptible cells that can process S protein of SARS-CoV2 to generate S1 and S2 subunits (Shang et al., 2020; Sungnak et al., 2020; V'kovski et al., 2020). The cleavage of S protein could facilitate the virus entry by promoting the interaction of its RBD with cellular ACE2 receptors (Qiao and DeLa Cruz, 2020; Shang et al., 2020). SARS-CoV2 generated variants predominantly target the RBD of S protein because such mutations are likely to be efficiently selected under the immune pressure to provide the virus a fitness

advantage (Baric, 2020; Weisblum et al., 2020). Given that the variants carrying extensive mutations in the CSP of SARS-CoV2 are not reported, such sites could conceivably be critical in enhancing the infectivity. We, therefore, considered targeting such a site by the sdAb and observed their utility in neutralizing not only the SARS-CoV2 surrogate virus but also two completely unrelated viruses. We further considered using such sdAbs as valuable tools in deciphering the intracellular events in the viral biogenesis. Both the antibodies when expressed intracellularly dramatically blocked the virus production (Figure 5). The fine cellular and molecular details of such processes in interfering with the trafficking pattern and the assembly of virions are being currently investigated but our data suggested for altered processing pattern as well as the sequestration of the S protein by such antibodies in ER followed by degradation. Therefore, the S protein become unavailable for the virion assembly (Wagner and Rothbauer, 2020; Zhang et al., 2020).

Although the infectivity and transmissibility of currently circulating SARS-CoV2 is more as compared to the previous coronaviruses that caused pandemics, the overall number of cases with severe disease are relatively lower. Several issues remain unresolved that can account for the varied disease outcome of COVID-19 in infected individuals. Some of the known factors responsible for disease outcome include the age of the host when infected, comorbidities as well as genetic factors such as the impairment with type I IFN pathways (Rouse and Sehrawat, 2010). Pre-existing antibodies specific to polybasic CS induced by a prior exposure of HSV1 or other viruses might offer protection against the COVID-19. We demonstrate SARS-CoV2 neutralizing antibodies in anti-HSV1 sera but data from HSV1 infection in human population could provide additional conclusive evidence for their differential response pattern to COVID-19. Such polybasic CS occur in many viruses and microbial products and their recognition by B cells and specific antibodies to such sites could offer some level of cross-protection against SARS-CoV2 in most individuals. Furthermore, vaccines against measles virus, a morbillivirus, are routinely included in childhood immunization programs. The cross-reactive epitopes present in the polybasic sites of fusion protein (F protein) of measles virus (RRHKR) might induce antibody response to provide cross- protection against SARS-CoV2. This could partly help explain why children are less susceptible to develop severe COVID-19. As no approved SARS-CoV2 vaccines are available for children for a worldwide rollout, uninterrupted routine immunization against viruses such as measles, mumps and rubella might be conceived as a strategy to reduce their susceptibility to develop severe reactions following COVID-19 infection. Such vaccination could elicit both non-specific as well as cross-reactive antibodies against SARS-CoV2. The relative abundance of cross-reactive antibodies and possibly T cell response could finally shape COVID-19 outcome. Although we provide evidence on such cross-reactions focusing on polybasic sites, further analysis in human population would be valuable.

Limitations of the study

Anti-dengue virus (DNV) sdAb used as a control in the study has not been extensively characterized. However, our preliminary data clearly points towards its specificity to the virus. We have not tested the therapeutic potential of the described sdAbs in neutralizing the authentic SARS-CoV2 but the neutralization of two other viruses (PPRV and HSV1) was demonstrated *in vivo* as well as *in vitro* by anti-CSP sdAb. Nonetheless, we provide a platform for the *in vitro* analysis of SARS-CoV2-S protein expressing pseudoviruses assembly, and its neutralization by selected sdAbs. Furthermore, we have shown the effects of intracellularly expressed intrabodies in the biogenesis of such virions that could add to the growing list of resources and approaches available to decipher fine molecular and biochemical investigations.

STAR★METHODS

Detailed methods are provided in the online version of this paper and include the following:

- KEY RESOURCES TABLE
- RESOURCE AVAILABILITY
  - Lead contact
  - Materials availability
  - Data and code availability
- EXPERIMENTAL MODEL AND SUBJECT DETAILS
  - Mice and viruses
- METHOD DETAILS
  - Selection of anti-CSP sdAb from a phage display library by biopanning
  - Cloning and expression of sdAb

SUPPLEMENTAL INFORMATION

Supplemental information can be found online at https://doi.org/10.1016/j.isci.2022.104549.

ACKNOWLEDGMENTS

We thank Dr Kartik Chandran and Dr Rohit K Jangra of Albert Einstein college of Medicine, New York and Dr Jason McLellan of the University of Texas, Austin for sharing critical reagents for the work. We also thank Dr Indranil Banerjee and Dr Anand K Bachhawat for discussion and additional support for the completion of work. The help provided by Dr Barry T Rouse of the University of Tennessee, Knoxville, USA in editing the MS is much appreciated.

Sudhakar Singh received fellowship from Indian Council of Medical Research., Y.J.S., received fellowship from Council of Scientific & Industrial Research, and S.D., A.T., R.S., K.B., A.J., received their fellowships from Intramural funds from IISER Mohali. The study was supported partly by intramural funding from IISER Mohali, extramural grants from DBT (BT/PR20283/BBE/117/2016) and IPA/2021/000136 to Sharvan Sehrawat. Sudhakar Singh, Surbhi Dahiya and Sharvan Sehrawat are co-inventors on a pending patent application (202211016615).

AUTHOR CONTRIBUTIONS

Conceptualization: S.S. and S.D.; Methodology: S.S., S.D., Y.J.S., K.B., A.J., R.S., A.D., A.T.; Writing- Original draft: S.S. and S.D.; Writing- Review and Editing: S.S., S.D., Y.J.S., K.B., A.J., R.S., A.D., A.T.; Visualization & Data Presentation: S.S., S.D., Y.J.S., K.B., A.J., R.S., A.D., A.T.; Data curation & formal analysis: S.S., S.D., Y.J.S., K.B., A.J., R.S., A.D., A.T.; Supervision: S. Sehrawat; Funding acquisition: S. Sehrawat.

DECLARATION OF INTERESTS

The authors declare no competing interest.

Received: February 22, 2022
Revised: May 8, 2022
Accepted: June 2, 2022
Published: July 15, 2022

REFERENCES

Baric, R.S. (2020). Emergence of a highly fit SARS-CoV-2 variant. N. Engl. J. Med. *383*, 2684–2686. https://doi.org/10.1056/nejmcibr2032888.

Braun, E., and Sauter, D. (2019). Furin-mediated protein processing in infectious diseases and cancer. Clin. Transl. Immunol. *8*, e1073. https://doi.org/10.1002/cti2.1073.

Buchrieser, J., Dufloo, J., Hubert, M., Monel, B., Planas, D., Rajah, M.M., Planchais, C., Porrot, F., Guivel-Benhassine, F., Van der Werf, S., et al. (2020). Syncytia formation by SARS-CoV-2-infected cells. EMBO J. *39*, e106267. https://doi.org/10.15252/embj.2020106267.

Casadevall, A., and Pirofski, L.A. (2020). The convalescent sera option for containing COVID-19. J. Clin. Invest. *130*, 1545–1548. https://doi.org/10.1172/jci138003.

Crawford, K.H.D., Eguia, R., Dingens, A.S., Loes, A.N., Malone, K.D., Wolf, C.R., Chu, H.Y., Tortorici, M.A., Veesler, D., Murphy, M., et al. (2020). Protocol and reagents for pseudotyping lentiviral particles with SARS-CoV-2 spike protein for neutralization assays. Viruses *12*, 513. https://doi.org/10.3390/v12050513.

de Breyne, S., Vindry, C., Guillin, O., Condé, L., Mure, F., Gruffat, H., Chavatte, L., and Ohlmann, T. (2020). Translational control of coronaviruses. Nucleic Acids Res. *48*, 12502–12522. https://doi.org/10.1093/nar/gkaa1116.

Dubey, A., Dahiya, S., Rouse, B.T., and Sehrawat, S. (2020). Perspective: reducing SARS-CoV2 infectivity and its associated immunopathology. Front. Immunol. *11*, 581076. https://doi.org/10.3389/fimmu.2020.581076.

Dumoulin, M., Conrath, K., Van Meirhaeghe, A., Meersman, F., Heremans, K., Frenken, L.G.J., Muyldermans, S., Wyns, L., and Matagne, A. (2009). Single-domain antibody fragments with high conformational stability. Protein Sci. *11*, 500–515. https://doi.org/10.1110/ps.34602.

Garcia-Beltran, W.F., Lam, E.C., St. Denis, K., Nitido, A.D., Garcia, Z.H., Hauser, B.M., Feldman, J., Pavlovic, M.N., Gregory, D.J., Poznansky, M.C., et al. (2021). Multiple SARS-CoV-2 variants escape neutralization by vaccine-induced humoral immunity. Cell *184*, 2372–2383.e9. https://doi.org/10.1016/j.cell.2021.03.013.

Hoffmann, M., Kleine-Weber, H., and Pöhlmann, S. (2020). A multibasic cleavage site in the spike protein of SARS-CoV-2 is essential for infection of human lung cells. Mol. Cell. *78*, 779–784.e5. https://doi.org/10.1016/j.molcel.2020.04.022.

Hsieh, C.L., Goldsmith, J.A., Schaub, J.M., DiVenere, A.M., Kuo, H.C., Javanmardi, K., Le, K.C., Wrapp, D., Lee, A.G., Liu, Y., et al. (2020). Structure-based design of prefusion-stabilized SARS-CoV-2 spikes. Science *369*, 1501–1505. https://doi.org/10.1126/science.abd0826.

Hu, B., Guo, H., Zhou, P., and Shi, Z.L. (2020). Characteristics of SARS-CoV-2 and COVID-19. Nat. Rev. Microbiol. *19*, 141–154. https://doi.org/10.1038/s41579-020-00459-7.

Huang, Y., Yang, C., Xu, X.F., Xu, W., and Liu, S.W. (2020). Structural and functional properties of SARS-CoV-2 spike protein: potential antivirus drug development for COVID-19. Acta Pharmacol. Sin. *41*, 1141–1149. https://doi.org/10.1038/s41401-020-0485-4.

Fagan, P.K., Reinscheid, D., Gottschalk, B., and Chhatwal, G.S. (2001). Identification and characterization of a novel secreted immunoglobulin binding protein from group A Streptococcus. Infect. Immun. *69*, 4851–4857. https://doi.org/10.1128/iai.69.8.4851-4857.2001.

Ingram, J.R., Schmidt, F.I., and Ploegh, H.L. (2018). Exploiting nanobodies' singular traits. Annu. Rev. Immunol. *36*, 695–715. https://doi.org/10.1146/annurev-immunol-042617-053327.

Izaguirre, G. (2019). The proteolytic regulation of virus cell entry by furin and other proprotein convertases. Viruses *11*, 837. https://doi.org/10.3390/v11090837.

Jackson, L.A., Anderson, E.J., Rouphael, N.G., Roberts, P.C., Makhene, M., Coler, R.N., McCullough, M.P., Chappell, J.D., Denison, M.R., Stevens, L.J., et al. (2020). An mRNA vaccine against SARS-CoV-2 — preliminary report. N. Engl. J. Med. *383*, 1920–1931. https://doi.org/10.1056/nejmoa2022483.

Jaimes, J.A., Millet, J.K., and Whittaker, G.R. (2020). Proteolytic cleavage of the SARS-CoV-2 spike protein and the role of the novel S1/S2 site. iScience *23*, 101212. https://doi.org/10.1016/j.isci.2020.101212.

Johnson, B.A., Xie, X., Bailey, A.L., Kalveram, B., Lokugamage, K.G., Muruato, A., Zou, J., Zhang, X., Juelich, T., Smith, J.K., et al. (2021). Loss of furin cleavage site attenuates SARS-CoV-2 pathogenesis. Nature *591*, 293–299. https://doi.org/10.1038/s41586-021-03237-4.

Kaur, M., Dubey, A., Khatri, M., and Sehrawat, S. (2019). Secretory PLA2 specific single domain antibody neutralizes Russell viper venom induced cellular and organismal toxicity. Toxicon *172*, 15–18. https://doi.org/10.1016/j.toxicon.2019.10.240.

Lee, C.Y.-P., Carissimo, G., Chen, Z., Lum, F.-M., Abu Bakar, F., Rajarethinam, R., Teo, T.-H., Torres-Ruesta, A., Renia, L., and Ng, L.F. (2020). Type I interferon shapes the quantity and quality of the anti-Zika virus antibody response. Clin. Transl. Immunol. *9*, e1126. https://doi.org/10.1002/cti2.1126.

Maggi, M., and Scotti, C. (2017). Enhanced expression and purification of camelid single domain VHH antibodies from classical inclusion bodies. Protein Expr. Purif. *136*, 39–44. https://doi.org/10.1016/j.pep.2017.02.007.

de Marco, A. (2011). Biotechnological applications of recombinant single-domain antibody fragments. Microb. Cell Factories *10*, 44. https://doi.org/10.1186/1475-2859-10-44.

Ming Hsu, C.Y., and Uluda Ğ, H. (2012). A simple and rapid nonviral approach to efficiently transfect primary tissue-derived cells using polyethylenimine. Nat. Protoc. *7*, 935–945. https://doi.org/10.1038/nprot.2012.038.

Ou, X., Liu, Y., Lei, X., Li, P., Mi, D., Ren, L., Guo, L., Guo, R., Chen, T., Hu, J., et al. (2020). Characterization of spike glycoprotein of SARS-CoV-2 on virus entry and its immune cross-reactivity with SARS-CoV. Nat. Commun. *11*, 1620. https://doi.org/10.1038/s41467-020-15562-9.

Papa, G., Mallery, D.L., Albecka, A., Welch, L.G., Cattin-Ortolá, J., Luptak, J., Paul, D., McMahon, H.T., Goodfellow, I.G., Carter, A., et al. (2021). Furin cleavage of SARS-CoV-2 Spike promotes but is not essential for infection and cell-cell fusion. PLoS Pathog. *17*, e1009246. https://doi.org/10.1371/journal.ppat.1009246.

Peacock, T.P., Goldhill, D.H., Zhou, J., Baillon, L., Frise, R., Swann, O.C., Kugathasan, R., Penn, R., Brown, J.C., Sanchez-David, R.Y., et al. (2021). The furin cleavage site in the SARS-CoV-2 spike protein is required for transmission in ferrets. Nat. Microbiol. *6*, 899–909. https://doi.org/10.1038/s41564-021-00908-w.

Polack, F.P., Thomas, S.J., Kitchin, N., Absalon, J., Gurtman, A., Lockhart, S., Perez, J.L., Pérez Marc, G., Moreira, E.D., Zerbini, C., et al. (2020). Safety and efficacy of the BNT162b2 mRNA covid-19 vaccine. N. Engl. J. Med. *383*, 2603–2615. https://doi.org/10.1056/nejmoa2034577.

Qiao, B., and De La Cruz, M.O. (2020). Enhanced binding of SARS-CoV-2 spike protein to receptor by distal polybasic cleavage sites. ACS Nano *14*, 10616–10623. https://doi.org/10.1021/acsnano.0c04798.

Ramakrishna, C., Ferraioli, A., Calle, A., Nguyen, T.K., Openshaw, H., Lundberg, P.S., Lomonte, P., and Cantin, E.M. (2015). Establishment of HSV1 latency in immunodeficient mice facilitates efficient in vivo reactivation. PLoS Pathog. *11*, e1004730. https://doi.org/10.1371/journal.ppat.1004730.

Rottier, P.J., Horzinek, M.C., and van der Zeijst, B.A. (1981). Viral protein synthesis in mouse hepatitis virus strain A59-infected cells: effect of tunicamycin. J. Virol. *40*, 350–357. https://doi.org/10.1128/jvi.40.2.350-357.1981.

Rouse, B.T., and Sehrawat, S. (2010). Immunity and immunopathology to viruses: What decides the outcome? Nat. Rev. Immunol. *10*, 514–526. https://doi.org/10.1038/nri2802.

Salvatori, G., Luberto, L., Maffei, M., Aurisicchio, L., Aurisicchio, L., Roscilli, G., Roscilli, G., Palombo, F., Marra, E., and Marra, E. (2020). SARS-CoV-2 spike protein: an optimal immunological target for vaccines. J. Transl. Med. *18*, 222. https://doi.org/10.1186/s12967-020-02392-y.

Schrauwen, E.J.A., Herfst, S., Leijten, L.M., van Run, P., Bestebroer, T.M., Linster, M., Bodewes, R., Kreijtz, J.H.C.M., Rimmelzwaan, G.F., Osterhaus, A.D.M.E., et al. (2012). The multibasic cleavage site in H5N1 virus is critical for systemic spread along the olfactory and hematogenous routes in ferrets. J. Virol. *86*, 3975–3984. https://doi.org/10.1128/jvi.06828-11.

Sehrawat, S., Reddy, P.B.J., Rajasagi, N., Suryawanshi, A., Hirashima, M., and Rouse, B.T. (2010). Galectin-9/TIM-3 interaction regulates virus-specific primary and memory CD8+ T cell response. PLoS Pathog. *6*, e1000882. https://doi.org/10.1371/journal.ppat.1000882.

Sehrawat, S., and Rouse, B.T. (2020). Does the hygiene hypothesis apply to COVID-19 susceptibility? Microbes infect. *22*, 400–402. https://doi.org/10.1016/j.micinf.2020.07.002.

Shang, J., Wan, Y., Luo, C., Ye, G., Geng, Q., Auerbach, A., and Li, F. (2020). Cell entry mechanisms of SARS-CoV-2. Proc. Natl. Acad. Sci. USA *117*, 11727–11734. https://doi.org/10.1073/pnas.2003138117.

Sharma, Y., Sarkar, R., Jain, A., Singh, S., Shekhar, C., Shanmugam, C., Dhanavelu, M., Tembhurne, P., Kaul, R., and Sehrawat, S. (2021). A mouse model of PPRV infection for elucidating protective and pathological roles of immune cells. Front. Immunol. *12*, 630307. https://doi.org/10.3389/fimmu.2021.630307.

Sungnak, W., Huang, N., Bécavin, C., Berg, M., Queen, R., Litvinukova, M., Talavera-López, C., Maatz, H., Reichart, D., Sampaziotis, F., et al. (2020). SARS-CoV-2 entry factors are highly expressed in nasal epithelial cells together with innate immune genes. Nat. Med. *26*, 681–687. https://doi.org/10.1038/s41591-020-0868-6.

Swanson, C.L., Wilson, T.J., Strauch, P., Colonna, M., Pelanda, R., and Torres, R.M. (2010). Type I IFN enhances follicular B cell contribution to the T cell-independent antibody response. J. Exp. Med. *207*, 1485–1500. https://doi.org/10.1084/jem.20092695.

V'kovski, P., Kratzel, A., Steiner, S., Stalder, H., and Thiel, V. (2020). Coronavirus biology and replication: implications for SARS-CoV-2. Nat. Rev. Microbiol. *19*, 155–170. https://doi.org/10.1038/s41579-020-00468-6.

Wagner, T.R., and Rothbauer, U. (2020). Nanobodiesright in the middle: intrabodies as toolbox to visualize and modulate antigens in the living cell. Biomolecules *10*, 1701. https://doi.org/10.3390/biom10121701.

Weisblum, Y., Schmidt, F., Zhang, F., DaSilva, J., Poston, D., Lorenzi, J.C.C., Muecksch, F., Rutkowska, M., Hoffmann, H.H., Michailidis, E., et al. (2020). Escape from neutralizing antibodies by SARS-CoV-2 spike protein variants. Elife *9*, e61312. https://doi.org/10.7554/elife.61312.

Winstone, H., Lista, M.J., Reid, A.C., Bouton, C., Pickering, S., Galao, R.P., Kerridge, C., Doores, K.J., Swanson, C.M., and Neil, S.J.D. (2021). The polybasic cleavage site in SARS-CoV-2 spike modulates viral sensitivity to type I interferon and IFITM2. J. Virol. *95*, e02422-20. https://doi.org/10.1128/jvi.02422-20.

Wrapp, D., De Vlieger, D., Corbett, K.S., Torres, G.M., Wang, N., Van Breedam, W., et al. (2020). Structural basis for potent neutralization of betacoronaviruses by single-domain camelid antibodies. Cell *181*. 1004–15. https://doi.org/10.1016/j.cell.2020.04.031.

Xia, S., Liu, M., Wang, C., Xu, W., Lan, Q., Feng, S., Qi, F., Bao, L., Du, L., Liu, S., et al. (2020). Inhibition of SARS-CoV-2 (previously 2019-nCoV) infection by a highly potent pan-coronavirus fusion inhibitor targeting its spike protein that harbors a high capacity to mediate membrane fusion. Cell Res. *30*, 343–355. https://doi.org/10.1038/s41422-020-0305-x.

Yu, X., Xu, Q., Wu, Y., Jiang, H., Wei, W., Zulipikaer, A., Guo, Y., Jirimutu, and Chen, J. (2020). Nanobodies derived from Camelids represent versatile biomolecules for biomedical applications. Biomater. Sci. *8*, 3559–3573. https://doi.org/10.1039/d0bm00574f.

Zhang, C., Ötjengerdes, R.M., Roewe, J., Mejias, R., and Marschall, A.L.J. (2020). Applying antibodies inside cells: principles and recent advances in neurobiology, virology and oncology. BioDrugs *34*, 435–462. https://doi.org/10.1007/s40259-020-00419-w.

Zhao, G., Du, L., Ma, C., Li, Y., Li, L., Poon, V.K., Wang, L., Yu, F., Zheng, B.J., Jiang, S., and Zhou, Y. (2013). A safe and convenient pseudovirus-based inhibition assay to detect neutralizing antibodies and screen for viral entry inhibitors against the novel human coronavirus MERS-CoV. Virol. J. *10*, 266. https://doi.org/10.1186/1743-422x-10-266.

STAR★METHODS

KEY RESOURCES TABLE

REAGENT or RESOURCE	SOURCE	IDENTIFIER
Antibodies		
anti-c-myc tag antibody	SCBT	Cat#9E10; RRID:AB_627268
streptavidin APC	BioLegend	Cat#405207
Mouse 6X(His) tag	Invitrogen	Cat#37-2900; RRID:AB_2533309
Alkaline phosphatase conjugated goat anti-mouse IgG	Sigma	Cat#A3562; RRID:AB_258091
anti-ubiquitin antibody	SCBT	Cat#Sc8017; RRID:B_628423
anti-GAPDH antibody	Invitrogen	Cat# MA5-15738; RRID:AB_10977387
Golgin Rabbit	Sigma	Cat# PA5-52841; RRID:AB_2642110
Calnexin Rabbit	CST, Beverly, Massachusetts, USA	Cat# 2679; RRID:AB_2228381
Alexa Fluor 647 anti-mouse in Goat	Thermofisher Scientific	Cat# A21235; RRID:AB_2535804
Alexa fluor 568 anti-Rabbit in Goat	Thermofisher Scientific	Cat#A11036; RRID:AB_10563566
Hoechst stain	Thermofisher Scientific	62249
Steptavidin HRP	life technology	SNN1004
Anti-Flag mouse antibody	Sigma	Cat# F1804-50UG; RRID:AB_262044
Chemicals, peptides, and recombinant proteins		
Tunicamycin	Sigma	T7765-5MG
PVDF Membrane	BioRad	Cat#1620177
Trypsin	HiMedia	59427C-500ML
Bovine Serum Albumin	Himedia	GRM105-100G
Ni- NTA beads	G Biosciences	Cat#786940
TMB substrate (ELISA)	BD	Cat#555214
FemtoLUCENT plus AP kit	G Biosciences	Cat#786-10AP
PEI Branched	Sigma	408727-100mL
BamHI	NEB	R3136S
XbaI	NEB	R0145S
NcoI	NEB	R3193S
NotI	NEB	R3189S
MG132	Sigma	474787
Ni-NTA probes	ForteBio	18-5101
Clarity Western ECL substrate	Bio-Rad	Cat#170-5060
pNPP substrate	Sigma	71768-25G
DMEM	Gibco	10566-016-500mL
RPMI	Gibco	A10491-01 500mL
Fetal Bovine Serum	Gibco	10270106- 500 mL
Recombinant DNA constructs		
WT SARS-CoV-2 S Plasmid	Dr. Jason McLellan (University of Texas) (Wrapp et al., 2020)	https://doi.org/10.1126/science.abb2507
Mutated SARS-CoV-2 S Plasmid	Dr. Jason McLellan	
pCMVR8.74	Dr. Indranil Banerjee (IISER Mohali)	#22036
pMD2.G	Dr. Indranil Banerjee	#12259
Pcmv14-3X-FLAG-SARS-CoV-2S	Addgene	#145780

(*Continued on next page*)

Continued

REAGENT or RESOURCE	SOURCE	IDENTIFIER
pLenti GFP	Addgene	#17448
Tat1b and Rev 1b	SARS-Related Coronavirus 2, Wuhan-Hu-1 spike-pseudotyped lentiviral kit	NR-52948
YBNT (modified pet 22b)	Novagen	pET22b^{+}
RBD-pET22b	In-house generated	Used in this study
Anti-CSP-IB clone	In-house generated	Used in this study
Ant-RBD-IB clone	In-house generated	Used in this study
Experimental models: Cell lines		
HEK293T	ATCC	CRL-3216™
Vero E6 cells	Dr. Rajesh Ringe lab (IMTECH, CHANDIGARH)	NA
Vero cells	ATCC	CCL-81
Experimental models: Organisms/strains		
C57BL/6J WT	Jackson laboratory, USA	000664
IFNR KO (B6.Cg-*Ifngr1*^{tm1Agt} *Ifnar*$^{1tm1.2Ees}$/J)	Jackson laboratory, USA	029098
Rag1$^{-/-}$ B6 mice (B6.129S7-*Rag1*^{tm1Mom}/J)	Jackson laboratory, USA	002216
Oligonucleotides		
FP VHH FR1 pLenti:	GCC Biotech India	Sequence details are available in Table 1
FR4 C-Myc pLenti:	GCC Biotech India	Sequence details are available in Table 1
MKS-9 (VHH FP):	GCC Biotech India	Sequence details are available in Table 1
MKS-22 (VHH RP):	GCC Biotech India	Sequence details are available in Table 1
T7-FP:	GCC Biotech India	Sequence details are available in Table 1
T7-RP:	GCC Biotech India	Sequence details are available in Table 1
Software and algorithms		
FlowJoX software	BD Biosciences	https://www.flowjo.com/solutions/flowjo/downloads
Image J	NIH	https://imagej.nih.gov/ij/download.html
IEDB	NIAID	http://tools.iedb.org/main/bcell/
BLItz software	ForteBio	http://www.blitzmenow.com
GraphPad Prism 9	GraphPad	https://www.graphpad.com/scientific-software/prism/

RESOURCE AVAILABILITY

Lead contact

All the queries concerning reagents and resources could be directed to the lead contact (Sharvan Sehrawat, sharvan@iisermohali.ac.in).

Materials availability

The anti-CSP and anti-RBD sdAbs and their respective intrabody constructs generated as part of this study will be made available to investigators upon receiving request to the lead contact.

Data and code availability

This study did not generate any new codes. Any additional information required is available upon request to the lead contact.

EXPERIMENTAL MODEL AND SUBJECT DETAILS

Mice and viruses

C57BL/6J or WT, IFNR KO (B6.Cg-*Ifngr1*^{tm1Agt} *Ifnar*$^{1tm1.2Ees}$/J) and Rag1$^{-/-}$ B6 mice (B6.129S7-*Rag1*^{tm1Mom}/J) were purchased from Jackson Laboratory USA and maintained at IISER Mohali. All the experiments performed involve male mice of similar age group (6–8 weeks) maintained at similar housing condition at IISER Mohali. HSV1-KOS and PPRV, viruses used in this study were grown and titrated using Vero cells. All the experimental procedures were performed strictly in accordance with the protocol approved by the Institutional Animal Ethics Committee (IAEC), IISER Mohali, constituted under the aegis of committee for the purpose of control and supervision of experiments on animals (CPCSEA).

METHOD DETAILS

Selection of anti-CSP sdAb from a phage display library by biopanning

A previously generated phage display library of camelid V_HH was probed against the peptide encompassing the polybasic cleavage site of SARS-CoV2 S protein (Kaur et al., 2019). Competent TG1 bacterial cells were cultured in glucose supplemented 2xYT medium until an OD_{600} value of 0.4 was reached. TG1 cells were then infected with helper phage M13K07 under static conditions at 30°C for 40 min. Thereafter, the medium was supplemented with kanamycin (50 μg/mL) and grown overnight for the multiplication of phages. Bacterial cells were then pelleted at low temperature to collect supernatant. The supernatant was then precipitated using 20% polyethylene glycol (PEG) and 0.5M NaCl to obtain helper phages, used for infecting recombinant TG1 cells harbouring V_HH sequences. Helper phage particles expressing V_HH that were then used for bio-panning as described earlier (Kaur et al., 2019). Synthetic peptides predicted to be immunogenic for B cells were coated onto ELISA plates (50 μg/mL/well) at 4°C overnight followed by blocking the wells with 4% BSA for 2 h at room temperature (RT). ELISA plates were then washed three times with freshly prepared phosphate buffer saline with 1% Tween-20 (PBST). Subsequently, 10^{12} recombinant phages/well were added to the plate followed by incubation for 3 h at RT. Unbound phages were removed by extensive washings (25 times) with a freshly prepared PBST. The bound phages were then eluted using freshly prepared alkaline triethylamine acetate (TEA) buffer. The eluted phages were further enriched to enhance the affinity of peptide specific V_HH by performing second round of biopanning. The eluted phages were then used for infecting TG1 bacterial cells.

Cloning and expression of sdAb

Multiple bacterial colonies obtained were screened by colony PCR using V_HH specific primers as described earlier (Kaur et al., 2019). The positive clones were selected to isolate phagemids. The retrieved V_HH sequences were further sub-cloned into a modified pYBNT vector using MKS9 and MKS22 as forward and reverse primers respectively (primers sequences are mentioned in Table 1) containing a T7 promoter for bacterial expression (Kaur et al., 2019). Screening of clones were done through colony PCR using T7 forward and reverse primers. Out of the multiple colonies obtained, two clones were further processed for producing the sdAb against each of the target peptides from the RBD and the CS of SARS-CoV2 S protein. Clones were sequenced, expressed, purified, and characterized further. A primary bacterial culture of desired clones was propagated overnight in LB media supplemented with ampicillin (100 μg/mL) at 37°C followed by scaling up as one litre culture in shaking flasks until an OD_{600} of 0.4–0.6 was reached. The cultures were then induced with 1mM of IPTG for the induction of recombinant protein at 37°C in a shaking flask for 4 h. Thereafter the cultures were pelleted down by centrifugation at 8000rpm for 10 min at 4°C.

Purification of sdAb from inclusion bodies

To purify the recombinant protein from inclusion bodies, the pellets were first resuspended in lysis buffer containing 100mM Tris base and 10mM EDTA. The bacterial suspensions were sonicated on ice. Subsequently, the cells were centrifuged at 8000rpm for 10 min at 4°C to obtain the pellets which were then washed twice with wash buffer A (100mM Tris base, 10Mm EDTA, 1M NaCl, pH 8.0) and once with wash buffer B (100mM Tris Base, 10Mm EDTA, 1% v/v Triton 100; pH 8.0). The pellets were finally resuspended in denaturation buffer containing 100mM NaH_2PO_4, 10mM Tris-HCl, 8mM urea, pH 8.0 and kept at rotation for 18–20 h at 4°C. The denatured fractions were centrifuged at 5000 rpm at 4°C for 10 min to obtain the clear extract. The supernatant was subjected to Ni-NTA purification using HIS-trap columns pre-equilibrated with the denaturation buffer. The washing was done with 20mM imidazole in denaturation buffer (pH 8.0). The bound product was eluted using 400mM imidazole in denaturation buffer (pH 7.8). The final

protein yield was 20 mg/L. The protein thus obtained was mixed with an equal volume of guanidine solution (3M GuHCl, 10mM sodium acetate and 10mM EDTA, pH 4.2) and was refolded by a rapid dilution method using 100mM Tris, 1mM EDTA, 1mM GSH, 0.1mM GSSG, 400mM arginine as described earlier (Maggi and Scotti, 2017). The refolded fraction was then subjected to size exclusion chromatography using an S200 Hi-prep column (GE Healthcare, U.S.A) and two dominant peaks were obtained. The peaks obtained were pooled separately and spectral analysis was done using circular dichroism.

Measuring thermal and pH stability of sdAbs

To measure the effects of pH on the structural integrity of purified sdAb, the preparations were incubated in the buffers with varied pH values ranging from 2 to 13 for 10 min and CD spectral analysis was performed. Similarly, the effect of temperature on purified sdAb was analysed by performing thermal kinetics. The sdAb preparations were subjected to heating at different temperatures ranging from 20°C to 70°C and then cooling from 70°C to 20°C to measure their denaturation and renaturation kinetics.

Generation of SARS-CoV2 S pseudovirus

Plasmids encoding SARS-CoV-2 S protein were a kind gift from Dr. McLellan of the University of Texas, Austin and were described earlier(Hsieh et al., 2020). We used both WT SARS-CoV-2 S (RRAR, 682–685) and its CS mutated version (GSAS, 682-684) to generates pseudotype lentiviruses. Third generation lentiviral packaging vector, pCMVR8.74 and pMD2.G (VSV-G envelop vector) were also used. Plasmid encoding SARS-CoV2-spike protein, pCMV14-3X-FLAG-SARS-CoV-2S was from Addgene (#145780) and was described earlier(Ou et al., 2020). pLenti-GFP (Core with 5′ and -3′ LTR) was also from Addgene (#17448) and the plasmids containing Tat1b and Rev1b (SARS-Related Coronavirus 2, Wuhan-Hu-1 Spike-Pseudotyped Lentiviral Kit, NR-52948) were also obtained from BEI resources and were described earlier(Crawford et al., 2020). The above mentioned 5 plasmids, Spike construct (6μg), pCMVR8.74 (9μg), pLentiGFP (10.8μg), Tat-containing plasmid (6μg) and Rev plasmid (6μg) were mixed with 1:3 of PEI (1 mg/mL) (Ming Hsu and Uluda Ğ, 2012) in 5mL of serum free DMEM/petri-plate, followed by instant mixing by vortexing for 40 s. Above mixture was kept at RT for 15 min and co-transfected in HEK239T cells (Human Embryonic Kidney). The transfected HEK293T cells were used for the generating replication incompetent pseudotyped lentivirus (LV) expressing SARS-CoV2 S protein labelled as LV(CoV2-S) and VSV-G protein labelled as LV(VSV-G). The supernatants were collected at 72 h post transfection and centrifuged at 1000g to remove cell debris. The collected viral supernatant was concentrated with a solution, 1.2M NaCl and 40%(W/V) PEG-8000 on ice for 3-4 h followed by centrifugation at 3500g for 65 min. The precipitated virus pellets were dissolved in serum free medium, stored at 4°C and used within a few days-time. Modified Vero cells (Vero E6) originated from kidney epithelial cells of African green monkey were used for measuring the internalization using concentrated pseudoviruses. The cells were grown in 10% DMEM supplemented with 10× penicillin/streptomycin and maintained in a humidified CO_2 incubator at 37°C. Cellular infections with pseudoviruses were performed in serum free medium and after 24 h the culture media was replaced with complete DMEM. The cells were analysed for GFP expression 72 h post-infection by fluorescence microscopy using Nikon eclipse Ti. The cells were detached from the culture plates using 1mM PBS-EDTA, GFP expression was measured by flow cytometry. Vero E6 cells infected with bald particles or the LV (VSV-G) pseudovirus particles served as a control for such experiments.

Measuring neutralization of pseudoviruses by sdAb

Different dilutions of anti- cleavage site (anti-CSP) sdAb were used for measuring the internalization of LV(CoV2-S) pseudovirus particles by Vero E6 cells. For blocking experiments, we pre-incubated different concentrations of the sdAb (1 ng/mL, 10 ng/mL, 100 ng/mL, 500 ng/mL, 1 μg/mL, 5 μg/mL and 10 μg/mL) with 5 × 10^6 of either LV (CoV2-S) or LV(VSV-G) on ice for 1 h. Subsequently, the mix was added to 70–80% confluent Vero-E6 cells. After 24 h medium was replaced with a fresh complete medium. At different time points post-infection, the cells were analysed for GFP expression by fluorescent microscope and flow cytometry (BD Accuri).

In order to measure the specificity of anti-CSP sdAb, the CSP was added to it in different concentrations for 1 hr on ice. Anti-CSP sdAb or the mixtures was added to LV(CoV2-S) as described earlier. GFP expression was measured 72 h post-infection using fluorescence microscopy and flow cytometry.

In additional experiments, the anti-CSP antibody was added to trypsin-treated LV(CoV2-S) for 4hat 37°C, followed by incubation with anti-RBD sdAb (100 ng/mL) for 1 h on ice. The above mixture was applied to

Vero E6 cells and the infectivity was measured. Aliquots of the same sample was also processed by ELISA to analyse the trypsin-mediated cleavage of SARS-CoV2-S in the pseudovirus particles.

Evaluating the virus production by anti-S protein intrabodies

To produce sdAb as intrabodies we used a lentiviral vector (pLenti-GFP) in which anti-CSP and anti-RBD sdAb against cleavage site and RBD, respectively, were cloned in downstream of CMV promoter. Cloning strategy were as per the following cloning strategy, 5′LTR-CMV promoter-VHH - c-Myc-tag - e-GFP -3′-LTR. Anti-CSP and anti-RBD sdAb were amplified using the following primers FP VHH FR1 pLenti (containing *XbaI* restriction site) and FR4 c-Myc pLenti (primer with c-Myc tag attached to 3′ end of VHH containing *BamHI*), primers sequences are mentioned in the Table S1. The amplicon along with pLenti.GFP vector was digested using *BamHI* and *XbaI* for 5 hat 37°C followed by isopropanol precipitation, ligated in a vector to insert ratio of 1:5 and transformed to Stbl3 *E. coli* strain. Colonies confirmed through colony PCR and double digestion using given restriction sites. Positive clones were selected, grown in LB medium for overnight and the plasmid was isolated. Positive clones for anti-CSP or anti-RBD sdAb in fusion with c-Myc and GFP were co-transfected in HEK293 T cells along with other four plasmids (SARS CoV2 S construct, pCMVR8.9, Tat and Rev plasmids) for the production of the pseudovirus particles as described in a previous section. The culture supernatants were collected after 72 h of transfection. LV(CoV2-S) concentrated from the culture supernatants of the cells expressing anti-CSP and anti-RBD intrabodies. The induction of both the sdAb was measured by subjecting lysates of HEK293T cells to western blotting using anti-c-Myc tag antibodies. The concentrated supernatants were used to infect Vero E6 cells and the extent of infection was ascertained by fluorescence microscopy and flow cytometry. For control experiments, HEK293T cells were also transfected with all the above mentioned plasmids except for the SARS CoV2 S constructs which were replaced with VSV-G construct (pMD2.G) for expressing VSV-G glycoproteins.

In a separate experiment HEK293T cells were transfected in similar fashion as above mentioned to produce LV(Cov2-S) pseudoviruses, either in presence of anti-CSP intrabody or in presence of tunicamycin (2 μg/mL, added 24 h post-transfection), after 72 h of transfection supernatant were collected and concentrated and cell lysate were made. Supernatant and cell lysate were processed through indirect ELISA and western blotting respectively. Supernatant from the above experimental setup were also subjected to vero-E6 cells to measure the infective potential of LV(CoV2-S) pseudoviruses produced from different conditions.

In an additional experiment transfection was done in a similar way either in the presence of anti-CSP intrabody or tunicamycin (2 μg/mL). In some experiments, the transfected cells were 72 h later were treated with 5μM MG132 (proteasomal inhibitor) for 10 h before analysis. These cells were assessed for the expression and localization of S protein both intracellularly and that expressed on the surface using anti-RBD antibody. For surface staining these cells were first washed twice followed by incubation with biotin tagged anti-RBD antibody which were further detected using streptavidin-APC in flow cytometry. For the presence of intracellular spike cells were first fixed for 30 min on ice followed by permeabilized and then staining was performed in similar way as it was for surface staining. The relative intracellular and cell surface expression levels were calculated by subtracting.

Assessing the LV (CoV2-S) neutralization by HSV1 and PPRV infected mouse serum

Sera samples were collected between 10 to 15 days postinfection from C57BL/6J WT and IFNR KO (B6.Cg-*Ifngr1*^{tm1Agt} *Ifnar*$^{1tm1.2Ees}$/J) male mice (6–8 weeks) that were infected with HSV1 (5 × 10^5 PFU/footpad in 25μL volume) and PPRV (100 PFU/intraperitoneal), respectively. Different dilutions of the sera samples were pre-incubated with LV(CoV2-S) pseudovirus particles for 1 h on ice. Pre-incubated pseudovirus particles were used to assess the infectivity in Vero E6 cells. After 72 h cells were imaged using fluorescence microscopy and flow cytometry. The pre-immune sera samples collected from uninfected animals were used as a control.

In order to assess the contribution of polybasic CS-specific antibodies present in the anti-HSV1 or PPRV sera in neutralizing LV(CoV2-S), 1:100 dilution of sera samples were pre-incubated with different concentrations of CSP for 1 h on ice. The pre-incubated mixture was then added to LV(CoV2-S) pseudovirus particles for 1 h on ice and the mix was used to infect Vero E6 cells. After 72 h, GFP^{+ve} cells were observed using fluorescence microscopy and flow cytometry. Pre-immune sera from naïve mice were used as controls. Additionally, 100μg of CSP was coated overnight at 4°C. The respective serum samples were added to

these coated wells for 4 h at RT in order to deplete anti-CSP specific antibodies. The unbound serum was then used to measure the contribution of polybasic site specific antibodies in neutralising LV (CoV2-S).

Measuring the effect of specific sdAb in fusogenic activity

HEK293T cells were transfected with different plasmids to make LV (CoV2-S) pseudoviruses and Spike protein. After 72 h the generated pseudovirus particles were collected and the remaining transfected cells, HEK293T$^{+LV(CoV2\text{-}S)}$, were scrapped and used for cell fusion assay. The expression of the S protein in HEK293T cells was measured by their surface staining with both the sdAb using flow cytometry. HEK293T$^{+LV(CoV2\text{-}S)}$ were incubated with different concentrations of anti-CSP sdAb for 1h on ice followed by their co-culture with Vero E6 cells for 6 hrs at 37°C in humidified CO_2 incubator. The frequencies of fused cells were measured by fluorescence microscopy and flow cytometry(Xia et al., 2020). The fused cells would increase in size, therefore a flow cytometric analysis was performed.

Flow cytometry

After 72 h of infection with pseudovirues, Vero-E6 cells were treated with 1mM PBS-EDTA for 15 min at 37°C in CO_2 incubator and the cells were removed from 96 well-flat bottomed plates by gentle reverse pipetting. Cells were collected in 1.5mL micro-centrifuge tube, washed twice and acquired using flow cytometer (BD C6 Accuri) or BD FACSCalibur. The available data was analysed using flowJo X software (TreeStar).

Fluorescence microscopy

The cells were analysed for GFP expression 72 hrs post-infection (hpi) by fluorescence microscopy using Nikon eclipse Ti and all images were taken at 10× magnification. Analysis and scaling of all the taken images were done using ImageJ software.

Scanning electron microscopy

Field Emission Scanning Electron Microscope (FESEM) was used to measure the surface topography of LV(CoV2-S) and LV(VSV-G). Pseudoviral particles were spread and dehydrated on glass slide overnight, followed by coating with gold nanoparticle for providing conductivity to the samples and images were acquired using JEOL JSM-7600F FESEM.

Western blotting

To determine the specificity and immune reactivity of the sdAb with the SARS-CoV2 S protein, the polypeptides in the prepared samples of transfected HEK293T cells were resolved using SDS-PAGE, transferred to PVDF membrane and were immunoblotted with the sdAb containing 6×(HIS)-tag or their biotinylated versions after blocking of the membrane with 5% skim milk. Mouse anti- 6×(HIS) antibody (4A12E6) was from Invitrogen Rockford, USA). Alkaline phosphatase conjugated goat anti-mouse IgG (A3562) from Sigma, USA was used to develop the membranes. Since the spike construct contains a FLAG tag, immunoblotting was performed to detect the presence of spike protein in supernatant collected 24 h post transduction as well as in cell lysate of 72 h post transduced Vero E6 cells using anti-FLAG mouse antibody (F1804-50UG, USA). A secondary antibody anti-mouse IgG raised in goat and conjugated with alkaline phosphatase was used for the development of the blot.

Subsequently, for checking the ubiquitination status of the spike protein, the HEK293T cell lysate from transfected cells with 6xHIS tagged S construct in the presence of either tunicamycin or anti-CSP intrabody was first affinity purified using Ni-NTA beads and the eluted protein was visualised using anti-ubiquitin antibody. To ensure the effect was due to the expressed intrabody, the lysates were probed with anti-Myc antibody. Equal loading of the lysates was ensured using anti-GAPDH antibody. To detect all these primary antibodies, Goat anti-mouse IgG-alkaline phosphatase was used.

Indirect ELISA and competitive ELISA

Peptide against which the sdAb was biopanned was coated at a concentration of 50 μg/mL overnight at 4°C. The following day the wells were washed with 0.05% PBST and were blocked in 5% BSA in PBST for 2 h at RT and washed with 0.05% PBST. Thereafter, sdAb in different dilutions were incubated for 1.5 h at RT. For the detection of sdAb, anti-6x(HIS) antibody was added to these wells for 1 h at RT followed by washing and incubating with anti-mouse antibody conjugated alkaline phosphatase for 1.5 h. The plate was washed and developed with 100μL of pNpp substrate from Sigma Aldrich (1 mg/mL) in glycine buffer.

50μL of stop solution (3M NaOH) was added after the development of color and absorbance was taken at 405nm.

Biolayer interferometry (BLI)

BLI was performed to determine the binding kinetics of anti-CSP sdAb with the purified SARS-CoV2 S protein produced from transfected HEK293T cells (spike construct with 3× FLAG-tag) using BLItz System. For loading sdAb with 6×(HIS)-tagged), Ni-NTA probes (ForteBio) were used. 200μL of 250 μg/mL of both antibodies were loaded for 5 min and then washed with PBS to remove non-specific binding. Different concentrations of S protein were incubated for 5 min to measure the binding affinity with the immobilised anti-CSP sdAb and the dissociation kinetics was measured in PBS.

Confocal microscopy

HEK293T cells were seeded onto 1% gelatin coated (30min at 37ºC) coverslips. Approximately, 50% confluent cells were transfected with pLenti-GFP or with the modified pLenti GFP [anti-CS-myc-GFP as fusion product (Intrabody)] plasmid construct using PEI. After 24 h, re-transfection of the same cells was done with S construct plasmid. After 24 h of the S contruct transfection, tunicamycin (2 μg/mL) was added in those wells where HEK293T cells were transfected with pLentiGFP and S construct. After 24 h of tunicamycin treatment, all coverslips were fixed, stained and analysed by confocal microscopy. As a control untransfected HEK293T cells and only Anti-CS Intrabody expressing cells were taken. The cells were fixed with 4% para-formaldehyde for 15 min at room temperature and thereafter were washed three times with 1XPBS. Permeabilization of fixed cells were performed using ice cold 100% methanol kept at −20°C for 10 min. The cells were then washed once with 1XPBS. This was followed by blocking with 5% BSA and 0.3% triton X-100 in 1XPBS for 1 h at room temperature. The cells were then stained for 6xHIS tagged S protein using mouse anti- 6xHIS antibody (Invitrogen Rockford USA:4A12E6) at 1:100 dilution. For staining ER, rabbit anti-calnexin antibody (CST, Beverly, Massachusetts, USA: 52533S) at 1:100 dilution was used. For staining Golgi, rabbit anti-Golgin antibody (Sigma, USA: PA5-52841) at 1:100 dilution was used. All the antibodies were diluted in 1% BSA and 0.3% triton X-100 in 1XPBS. The cells were incubated with the respective primary antibody overnight at 4°C which then followed by washing with 1X PBS three times. For subsequent staining, the secondary antibodies were diluted in 1% BSA and 0.3% triton X-100 in 1XPBS. For detecting 6xHIS, goat anti-mouse Alexa fluor 647 ThermoFisher scientific, Waltham, Massachusetts: A21245) was used. For detecting both calnexin and golgin, goat anti-rabbit IgG Alexa Fluor 568 (ThermoFisher scientific, Waltham, Massachusetts: A11036) was used. For staining nucleus Hoechst stain (ThermoFisher scientific, Waltham, Massachusetts) was used along with secondary antibodies. The cells were incubated in secondary antibody for 1 h at room temperature and then washed with 1XPBS three times. For acquiring images using confocal microscopy, the coverslips containing the cells were fixed on slides using fluoromount-G (Sigma, USA) and left at room temperature for drying. All the confocal image stacks were obtained using a SP8 upright confocal microscope (Leica) and images were analysed using imageJ software.

Infection of mice with HSV1 and PPRV

C57BL/6J, IFNR KO (B6.Cg-*Ifngr1*^{tm1Agt} *Ifnar*$^{1tm1.2Ees}$/J) and Rag1$^{-/-}$ B6 mice (B6.129S7-*Rag1*^{tm1Mom}/J) male mice (6-8 weeks) were procured from Jackson Laboratory USA. The animals were housed and bred in the individual ventilated cages in the small animal facility for experimentation of Indian Institute of Science Education and Research (IISER), Mohali. Herpes simplex virus 1 (HSV1) and Pestis des Petitis Ruminants virus (PPRV) that have polybasic sites in their cellular entry mediators were used for mice infection to measure the neutralizing potential of anti-CSP sdAb as well as to collect specific anti-sera. For virus infection six to eight weeks old male (6-8 weeks) mice were used. RAG1$^{-/-}$ or IFNR$^{-/-}$ mice were infected in 5 × 10^5 pfu of HSV1 or 100pfu of PPRV or the same amount of viruses neutralized with 50ug of anti-CSP sdAb intraperitoneally. The infected animals were measured for their body weights postinfection and to collect different organs for virus load determination. In separate experiments, C57BL/6J and IFNR$^{-/-}$ male mice (6-8 weeks) were infected with 5 × 10^5 pfu of HSV1 (ocular route) and 100pfu of PPRV (intranasal route) titrated using Vero cells, respectively to collect anti-HSV1 and anti-PPRV sera. Anti-sera were used for measuring neutralization potential of pseudovirus expressing SARS-CoV2 S protein using Vero E6 cells. The animal experiments were performed strictly in accordance with the protocol approved by the Institutional Animal Ethics Committee (IAEC), IISER Mohali, constituted under the aegis of committee for the purpose of control and supervision of experiments on animals (CPCSEA).

ELISA for qualitative assessment of interaction between HSV1, PPRV and anti-CSP sdAb

100μL of concentrated HSV1-KOS and PPRV were coated overnight at 4°C. The following day wells were washed with 0.05% PBST and blocked in 5% BSA in PBS for 2 hrsat RT. After washings with PBST, 50 μg/mL of the biotinylated anti-CSP sdAb was added and the plated were incubated for 1.5 h at RT. For detection of bound sdAb, streptavidin-HRP was incubated for 30 min at RT. The plates were developed with 50μL of TMB substrate (BD biosciences) and the reaction was stopped by adding 50μL of 0.18M H_2SO_4 and absorbance was measured at 450nm.

Plaque assay for assessment of neutralizing ability of the anti-CSP sdAb and anti-polybasic sites antibody activity in anti-HSV1 and PPRV immune serum

Plaque assays were performed as previously reported (Sehrawat et al., 2010). Briefly, different dilutions of HSV1-KOS and PPRV were incubated on ice with 50 μg/mL of anti-CSP sdAb. The pre-incubated virus particles and the viruses treated similarly in the absence of anti-CSP sdAb were added to Vero cells for assessing the virus titres. Plaques were visualized by staining with crystal violet.

In a separate experiments, 1: 100 dilution of anti-HSV1 or PPRV sera samples collected from infected mice were pre-incubated with different concentrations of the CSP for one hour on ice. The adsorbed sera were then incubated with HSV1 and PPRV for one hour on ice. Untreated and treated viruses at 50 multiplicity of infection were assessed for their infectivity of Vero cells. The obtained plaques were visualized by using crystal violet and counted for PFU calculation. Pre-immune sera samples were used as controls.

Quantification of HSV1 in various organs

The quantification of HSV1 in lungs, kidney, liver and brain of the infected animals was performed as previously described (Sehrawat et al., 2010). Briefly, the mice were sacrificed at indicated times postinfection and the organs were stored in serum free RPMI at −80°C until further use. The tissues were disrupted by chopping with scissors and homogenized by using a homogenizer and centrifuged. The supernatant was used to assess viral titres on Vero cells. Finally, plaques were visualized after staining with crystal violet.

QUANTIFICATION AND STATISTICAL ANALYSIS

The data obtained was analysed by one way/Two way ANOVA and non-parametric t test. Data represents mean ± SEM and the level of statistical significance was determined as; ****$p < 0.0001$, ***$p < 0.001$, *$p < 0.01$ and *$p < 0.05$.